

Photometric and spectroscopic studies of the long period low mass ratio deep contact binary KN Per

XIN-YI GAO,¹ KAI LI,² YA-WEN CAI,¹ YA-NI GUO,² XING GAO,³ XI WANG,² SHI-PENG YIN,² FEI LIU,² AND
GUO-YOU SUN⁴

¹*SDU-ADU Joint Science College, Shandong University, Weihai, Shandong, 264209, China.*

²*Shandong Key Laboratory of Optical Astronomy and Solar-Terrestrial Environment,
School of Space Science and Physics,
Institute of Space Sciences, Shandong University,
Weihai, Shandong, 264209, China.*

³*Xinjiang Astronomical Observatory, 150 Science 1-Street, Urumqi 830011, China.*

⁴*Wenzhou Astronomical Association, Beibaixiang Town, Yueqing, Zhejiang, 325603, China.*

ABSTRACT

The photometric analysis and spectroscopic study of the long period low mass ratio deep contact binary KN Per were executed. The light curves of BV(RI)_c-band were from the Ningbo Bureau of Education and Xinjiang Observatory Telescope (NEXT) at the Xingming Observatory. Through the analysis of Wilson-Devinney (W-D) program, KN Per was found as an A-type low mass ratio deep contact binary ($q=0.236$, $f=53.4\%$). A cool spot applied on the primary component was introduced to explain the unequal maxima of the light curve. Based on the O-C analysis, we found that the rate of the increasing orbital period is $\dot{P} = 5.12 \pm (0.30) \times 10^{-7}$ d/yr, meaning the mass transfer from the secondary component to the primary one. By analyzing the spectroscopic data, we detected chromospheric activity emission line indicators, which is corresponding to the light-curve analysis. 71 long period ($P > 0.5$ days) contact binaries including our target were collected. The evolutionary states of all collected stars were investigated by the illustrations of mass-radius, mass-luminosity, and $\log M_T - \log J_o$. The relations of some physical parameters were also determined. With the instability parameters of KN Per, we determined that it is a stable contact binary system at present.

Keywords: binaries: close — binaries: eclipsing — binaries: spectroscopic — stars: individual: KN Per

1. INTRODUCTION

In the Galactic Disc, an abundant part (1 in 500) was considered to be contact binaries (Rucinski 2006). The contact binaries have two components, whose spectral types are from F to K (Rucinski 1993). A common convective envelope is existing in the contact binaries, which is shared by the primary and secondary stars (Lucy 1968). The contact binaries are divided into two types (Binnendijk 1970): A-type and W-type. For A-type binary, the surface temperature of the more massive star is higher than that of the less massive star, while W-type binary is quite the reverse. For contact binaries, the orbital periods are usually less than 0.7 days (Hilditch 2001).

Deep, low mass ratio overcontact binaries (DLMROBs) are a special kind of contact binaries, whose mass ratio are less than 0.25 and contact degree are more than 50% (Qian et al. 2005). They are thought to be at the late status in the evolution of close binary systems and may merge into fast rotating stars (Qian et al. 2008). Thus, DLMROBs may be the progenitors of blue straggler (Yang & Qian 2015), FK Com-type stars (Eggleton & Kiseleva-Eggleton 2001; Eggleton 2012) and luminous red novae (Kaczmarek et al. 2011; Stępień 2011; Tylenda et al. 2011; Zhu et al. 2016). Therefore, their photometric and spectrometric investigations are important.

Numerous contact binaries show chromospheric activity, because chromospheric activity usually exists in the kind of systems with spectral type later than F (Eker et al. 2008). Magnetic activities, which usually manifest themselves

as star spots, flares, and plages (Pribulla et al. 2003a), have a relationship with convective motions and rapid stellar rotation (Strassmeier 2009). For the photometric light curves, contact binaries will exhibit the O’Connell effect, the meaning of which is the two unequal maxima of the light curve (O’Connell 1951). For the spectroscopic data, there are special emission lines indicating chromospheric activity, such as Ca II H and K, Balmer series and Ca II triplet above the continuum (Pavlenko et al. 2018; Long et al. 2019; Zhang et al. 2020; Zheng et al. 2021).

KN Per was determined as a RR Lyrae star by Pinto & Romano (1976). They also derived the period of this target as 0.433224 days. A new period was determined by Eggen (1979), which is 0.232 days. Based on this period, Kemper (1982) proposed that KN Per is a δ Scuti star. The period was updated to be 0.433 days by Kholopov et al. (1985) and renewed as 0.866448 days by Schmidt (1991) based on the light curves in VR_c band. Schmidt & Reiswig (1993) also showed light curves in two bands (VR_c). Then, this target was classified into a faint δ Scuti star by Antonello & Mantegazza (1997). Finally, the first photometric analysis of light curves in VR_c band was carried out by Goderya et al. (1997) and a cool spot was applied on the secondary star. They found that KN Per is a DLMROB ($q=0.25$, $f=54.49\%$) with a period of 0.8664606 days. Recently, a O-C analysis was reported by Hu et al. (2018). They found that the orbital period shows a continuous increase. In this paper, new photometric and spectroscopic investigations of KN Per are presented.

2. OBSERVATIONS

2.1. Photometric Observations

The photometric observations of KN Per are from NEXT at Xingming Observation and other available light-curve databases, Transiting Exoplanet Survey Satellite (TESS) (Ricker et al. 2015), All-Sky Automated Survey for Supernovae (ASAS-SN) (Shappee et al. 2014; Jayasinghe et al. 2019) and Wide Angle Search for Planets (SuperWASP) (Butters et al. 2010).

The observations of NEXT at Xingming Observation were carried out on November 14, 16, 17, 19 and 20, 2019. The aperture of NEXT is 60 cm. A CCD camera with 2048×2048 pixels is included in NEXT, resulting a field of view around $22' \times 22'$. We adopted the standard Johnson-Cousin-Bessel $UBV(RI)_c$ filter system for the observation. All raw images were corrected for bias, dark and flat using the C-Munipack¹ program. C-Munipack is a software to process CCD photometric data. The CCD data were reduced using aperture photometry and differential photometry methods. Additionally, the magnitude differences among KN Per, the comparison and the check stars were obtained. Table 1 shows the photometric observation details of KN Per. The exposure times in B-band, V-band, R_c -band and I_c -band are 20s, 12s, 8s and 12s, respectively. The observing errors in $BV(RI)_c$ -band are shown in Table 2. We display the photometric data in Table 3 and show the light curves in Figure 1. The orbital phases can be determined by the following equation, using the period of Goderya et al. (1997),

$$T = T_0 + 0.8664606 \times E, \quad (1)$$

where T is the observed time, T_0 is a primary minimum obtained by the light curves and E is the epoch for corresponding T . For NEXT data, T are in HJD and T_0 is 2458802.11355. Except for NEXT, KN Per was also observed by TESS, ASAS-SN and SuperWASP. Sector 18 of TESS data has measured KN Per in a 30-minute cadence from November 4, 2019 to November 26, 2019. ASAS-SN has measured KN Per with the exposure time of 90s from January 15, 2015 to September 21, 2018, and SuperWASP has measured this target with the exposure time of 30s from August 13, 2004 to December 24, 2007. For TESS data, T in Equation (1) is in BJD and T_0 was 2458792.58670. For ASAS-SN and SuperWASP, we used different ephemerides. T in Equation (1) is in HJD and T_0 were 2458424.33330 and 2454022.65245, respectively. The deeper primary minimum was always chosen as phase zero. The three light curves of TESS, ASAS-SN and SuperWASP are shown in Figure 2.

2.2. Spectroscopic Observations

Having an aperture of 4 m, the Large Sky Area Multi-Object Fiber Spectroscopic Telescope (LAMOST) is a particular reflecting Schmidt telescope with a field of view of 5° and collects numerous stellar spectra (Luo et al. 2012). The range of the wavelength covered by LAMOST is from 3700\AA to 9000\AA (Cui et al. 2012; Du et al. 2016). The resolution is almost 1800 in the state of low resolution mode (Wang et al. 1996). 4000 fibers, located on the surface, improve the

¹ <http://c-munipack.sourceforge.net/>

Table 1. Observing details of KN Per

Stars	Name	α_{2000}	δ_{2000}	J	H	K
		h m s	° ' "	mag	mag	mag
KN Per	KN Per	03 22 35.853	+41 19 55.044	10.520	10.352	10.283
The comparison	2MASS 03231632+4120289	03 23 16.546	+41 20 29.143	9.047	8.388	8.279
The check	2MASS 03220492+4114261	03 22 05.145	+41 14 26.419	11.576	11.342	11.264

rate to acquire spectra greatly (Cui et al. 2012). For low resolution mode, two spectra of KN Per in 2012 and 2016 were found from Data Release 8². We display the spectral parameters in Table 4.

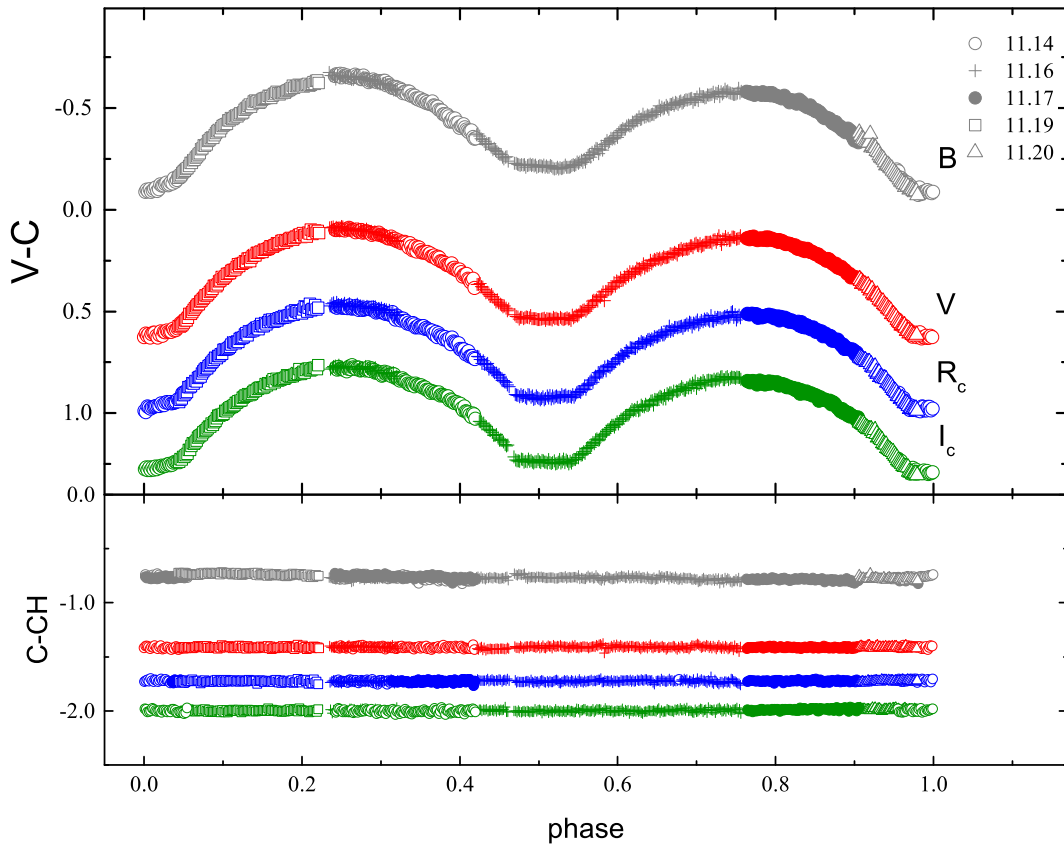


Figure 1. Four-band light curves of KN Per. The gray, red, blue and green symbols represent the light curves in B-band, V-band, R_c -band, I_c -band. The open circles, crosses, solid circles, hollow squares and hollow triangles represent the data on November 14, 16, 17, 19 and 20, 2019.

3. LIGHT-CURVE ANALYSIS

The effective temperature of the primary star, 7142 K, was determined by calculating the average value of the two temperatures shown in Table 4. The average temperature from LAMOST is the temperature of the system T_{eff} and not of the primary. This is usually assigned to the primary star to begin the modelling procedure i.e $T_1 \sim T_{eff}$. To ensure its reliability, the temperature obtained by the color indices was used to check it. We calculated the color

² <http://www.lamost.org/dr8/>

Table 2. Observing errors of KN Per

Band	Nov. 14	Nov. 16	Nov. 17	Nov. 19	Nov. 20
	mag	mag	mag	mag	mag
B	0.017	0.014	0.018	0.010	0.011
V	0.010	0.012	0.006	0.008	0.017
R_c	0.011	0.011	0.007	0.009	0.006
I_c	0.013	0.012	0.010	0.008	0.007

Table 3. The photometric data of KN Per obtained on November 14, 16, 17, 19 and 20, 2019

HJD _B	Δm_B	HJD _V	Δm_V	HJD _{R_c}	Δm_{R_c}	HJD _{I_c}	Δm_{I_c}
2400000+	mag	2400000+	mag	2400000+	mag	2400000+	mag
58802.07325	-0.198	58802.07369	0.538	58802.07405	0.900	58802.07437	1.224
58802.07486	-0.188	58802.07529	0.558	58802.07567	0.901	58802.07600	1.229
58802.07647	-0.159	58802.07692	0.567	58802.07729	0.923	58802.07764	1.233
58802.07812	-0.154	58802.07860	0.563	58802.07898	0.923	58802.07933	1.251
58802.07984	-0.145	58802.08026	0.567	58802.08066	0.926	58802.08100	1.257
...
58808.15838	-0.085	58808.15729	0.617	58808.15763	0.980	58808.15793	1.296
58808.15986	-0.089	58808.15878	0.623	58808.15912	0.977	58808.15941	1.296
58808.16133	-0.071	58808.16027	0.615	58808.16060	0.988	58808.16089	1.304

This table is available in its entirety in machine-readable form. A portion is shown here for guidance regarding its form and content.

Table 4. The Spectroscopic information of KN Per

Data	HJD	Phase	Exposures	Subclass	T_{eff}	log(g)	Radial velocity	H α (6564.61Å)
(d)	(d)		(s)		(K)		($km s^{-1}$)	
2012 Dec 25	2456289.11810	0.24393	1200	F0	7153.92	3.890	-64.92	0.195(0.010)
2016 Nov 16	2457709.12542	0.07332	1800	F0	7129.66	3.895	-24.12	0.153(0.010)

indices $B - V = 0.412$ mag, $g - r = 0.293$ mag and $J - K = 0.237$ mag from AAVSO Photometric All Sky Survey (APASS) (Henden et al. 2016) and Two Micron All-Sky Survey (2MASS)(Cutri et al. 2003). $E(B - V) = 0.130$ mag was obtained from a 3D Dust Map (Green et al. 2019) based on the distance 931.64 (0.02) pc from Gaia EDR3 (Gaia Collaboration et al. 2021). Finally, $(B - V)_0 = 0.282$ mag, $(g - r)_0 = 0.176$ mag and $(J - K)_0 = 0.173$ mag were determined. According to Table 5³ of Pecaut & Mamajek (2013), we obtained the corresponding temperatures (7200

³ http://www.pas.rochester.edu/~emamajek/EEM_dwarf_UBVIJHK_colors_Teff.txt

K, 7000 K and 7100 K) through the color indices. Then, the average value of them, 7100 K, was calculated. The difference between this result and the effective temperature obtained by LAMOST data is obviously small. Thus, the approximate value of LAMOST temperature 7140 K (± 20 K) was used in the following analysis.

Because the light curves determined from NEXT have four bands and a high photometric accuracy, NEXT data were used to determine the physical parameters by W-D program (Wilson & Devinney 1971; Wilson 1979, 1990, 1994). We derived q through the q -search method. The range of q is from 0.17 to 5.0. We set the step size as 0.01 in the range of $0.17 < q < 0.40$, and set the step size as 0.1 in the range of $0.4 < q < 5.0$. The following parameters are adjustable: the orbital inclination (i); the effective temperature of the less massive star (T_2); the luminosity of the more massive star (L_1) and the potential ($\Omega = \Omega_1 = \Omega_2$). We show the relation between q and mean residual in Figure 2. The minima of mean residual was seen at $q = 0.24$. Mean residual = $\sqrt{\frac{\sum_i W_i (O-C)_i^2}{N}}$ (N is the total number of all data).

Defining $q=0.24$ as the initial value and setting q adjustable, the analysis of the NEXT light curves was accomplished by W-D program. The theoretical light curves without spot are shown in Figure 3, which are represented by black lines. We found that the incompatibilities between the theoretical light curves and the observed light curves are obvious. Thus, we applied a cool spot on the primary star to further model the observed light curves. In this fitting process, the value of latitude was fixed at 90° . The theoretical light curves of spot model are shown in Figure 3 with red lines, which obviously fit the observed light curves very well. We should declare that the spotted models are not unique.

When we determined the temperature of the primary star, we ignored the existence of the surface brightness of the secondary star, which cannot be negligible. Thus, we assumed blackbody radiation to deal with this problem. 7140 K and 6860 K were assigned as the primary and secondary temperatures. We used the following equations to obtain the temperatures of both primary and secondary stars,

$$T_1 = (((1 + k^2)T_{eff}^4)/(1 + k^2(T_2'/T_1')^4))^{0.25}, \quad (2)$$

$$T_2 = T_1(T_2'/T_1'), \quad (3)$$

where T_{eff} is the effective temperature determined by LAMOST, k is the radius ratio and T_2'/T_1' is the temperature ratio (Zwitter et al. 2003; Christopoulou & Papageorgiou 2013). Then, the primary and secondary temperatures are 7200 K and 6917 K. The errors obtained by W-D program were too small to be true. To determine the more accurate physical parameters and their errors of KN Per, the Markov Chain Monte Carlo (MCMC) parameter search method by using PHOEBE (Prša & Zwitter 2005; Prša et al. 2016; Horvat et al. 2018; Conroy et al. 2020; Jones et al. 2020) was employed to analyze the NEXT data. The physical parameters obtained by W-D program were set as priors. We set walker as 24. The MCMC parameter search was run for 3000 steps for NEXT light curves and we deleted the first 1000 steps. The probability distributions of q , i , T_2 and $L_1/(L_1 + L_2)$ are shown in Figure 4. All the physical parameters are displayed in Table 5. The light curves of TESS, ASAS-SN and SuperWASP were analyzed by W-D program, respectively. We set the physical parameters determined from the NEXT light curves as the initial values. The value of latitude was still fixed at 90° . The theoretical light curves without spot and with a cool spot are all shown in Figure 3. Due to the high accuracy of the light curves observed by NEXT, the result of NEXT was chosen as the final result. The errors of the photometric solutions in Table 5 are formal and underestimated.

4. O-C DIAGRAM

We derived a total of 121 minimum timings to construct the O-C diagram. Minima calculated by us are shown as follows: 2 minimum timings determined from NEXT, 41 minimum moments from TESS, 3 minima obtained from the American Association of Variable Star Observers (AAVSO) and 26 minima from SuperWASP. In addition, 49 available moments were collected from the literature. We found that the two minimum timings, 2449697.6818 and 2449697.6823, from Goderya et al. (1997), are the same. Thus, the average value calculated by us was used in the following analysis. The photographic and visual minimum timings were not included in the following analysis due to their low accuracy. The minima from TESS are in BJD, the minimum timings from AAVSO are in JD, and the remaining are in HJD, which were turned into BJD through Time Utilities⁴. Table 6 shows the minimum timings. Based on the initial ephemeris presented by Pribulla et al. (2003a): $\text{Min.I} = 2449698.11390 + 0.8664593 \times E$, we calculated the values of O-C. Then, a linear fitting was applied to the O-C values. A new ephemeris was determined: $\text{Min.I} = 2449698.09710(\pm 0.00205) + 0.8664715(\pm 0.000003) \times E$. Finally, new O-C values were obtained by the above

⁴ <https://astrutils.astronomy.osu.edu/time/>

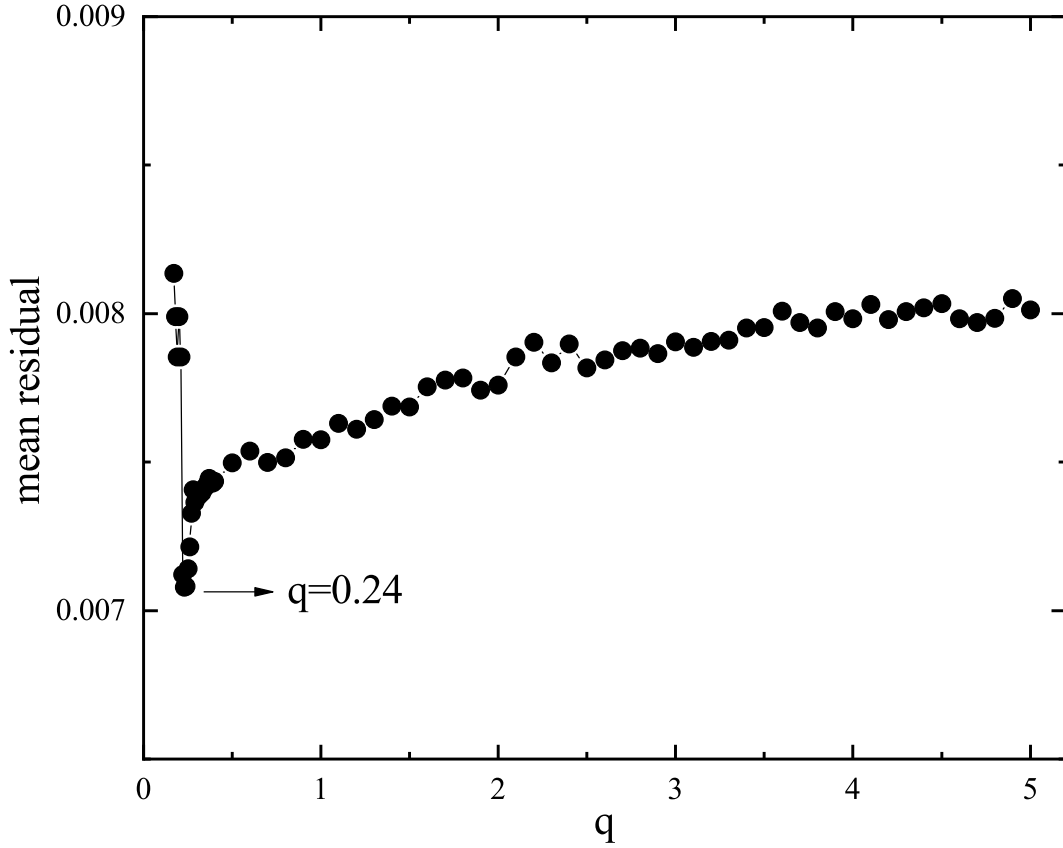


Figure 2. The relation between q and mean residual.

Table 5. Photometric solution of KN Per

	NEXT	TESS	ASAS-SN	SuperWASP
Primary temperature $T_1(K)$	7200	7200	7200	7200
Secondary temperature $T_2(K)$	6942^{+6}_{-4}	$6875(\pm 4)$	$6824(\pm 40)$	$6855(\pm 8)$
Mass ratio $q(M_2/M_1)$	$0.2360^{+0.0004}_{-0.0002}$	$0.2430(\pm 0.0007)$	$0.2356(\pm 0.0088)$	$0.2498(\pm 0.0016)$
Orbital inclination $i(\text{deg})$	$83.01^{+0.20}_{-0.22}$	$88.93(\pm 0.05)$	$80.24(\pm 0.08)$	$81.97(\pm 0.30)$
Modified dimensionless surface potential of star Ω	$2.259^{+0.011}_{-0.011}$	$2.242(\pm 0.002)$	$2.217(\pm 0.024)$	$2.256(\pm 0.005)$
Luminosity ratio $L_1/(L_1 + L_2)$ in TESS	-	$0.7538(\pm 0.0001)$	-	-
Luminosity ratio $L_1/(L_1 + L_2)$ in SuperWASP	-	-	-	$0.8028(\pm 0.0002)$
Luminosity ratio $L_1/(L_1 + L_2)$ in band B	$0.7679^{+0.0005}_{-0.0008}$	-	-	-
Luminosity ratio $L_1/(L_1 + L_2)$ in band V	$0.7732^{+0.0005}_{-0.0004}$	-	$0.8062(\pm 0.0002)$	-
Luminosity ratio $L_1/(L_1 + L_2)$ in band R_c	$0.7641^{+0.0005}_{-0.0004}$	-	-	-
Luminosity ratio $L_1/(L_1 + L_2)$ in band I_c	$0.7534^{+0.0006}_{-0.0004}$	-	-	-
Equal-volume radius of star 1 (relative to semimajor axis) r_1	$0.5326^{+0.0003}_{-0.0002}$	$0.5307(\pm 0.0004)$	$0.5445(\pm 0.0064)$	$0.5319(\pm 0.0011)$
Equal-volume radius of star 2 (relative to semimajor axis) r_2	$0.2958^{+0.0060}_{-0.0060}$	$0.3302(\pm 0.0023)$	$0.3029(\pm 0.0363)$	$0.2983(\pm 0.0052)$
Contact degree $f(\%)$	$53.4^{+4.4}_{-5.0}$	$61.9(\pm 1.3)$	$68.4(\pm 16.3)$	$60.9(\pm 3.0)$
Latitude $\theta(^{\circ})$	90.00	90.00	90.00	90.00
Longitude $\psi(^{\circ})$	$108.59^{+0.56}_{-0.88}$	$116.01(\pm 1.95)$	$118.15(\pm 7.63)$	$100.65(\pm 1.71)$
Spot radius $r(^{\circ})$	$29.36^{+0.20}_{-0.11}$	$18.13(\pm 0.09)$	$17.51(\pm 0.95)$	$19.39(\pm 0.18)$
Temperature factor T_f	$0.893^{+0.002}_{-0.001}$	$0.843(\pm 0.002)$	$0.856(\pm 0.022)$	$0.846(\pm 0.003)$

ephemeris and the O-C diagram is shown in Figure 5. The data shown in the red hollow points are data from the literature, the green hollow points are data from SuperWASP, the gray solid points represent the data of AAVSO, the blue hollow points are samples obtained from TESS and the red solid points are from NEXT. From this figure, the

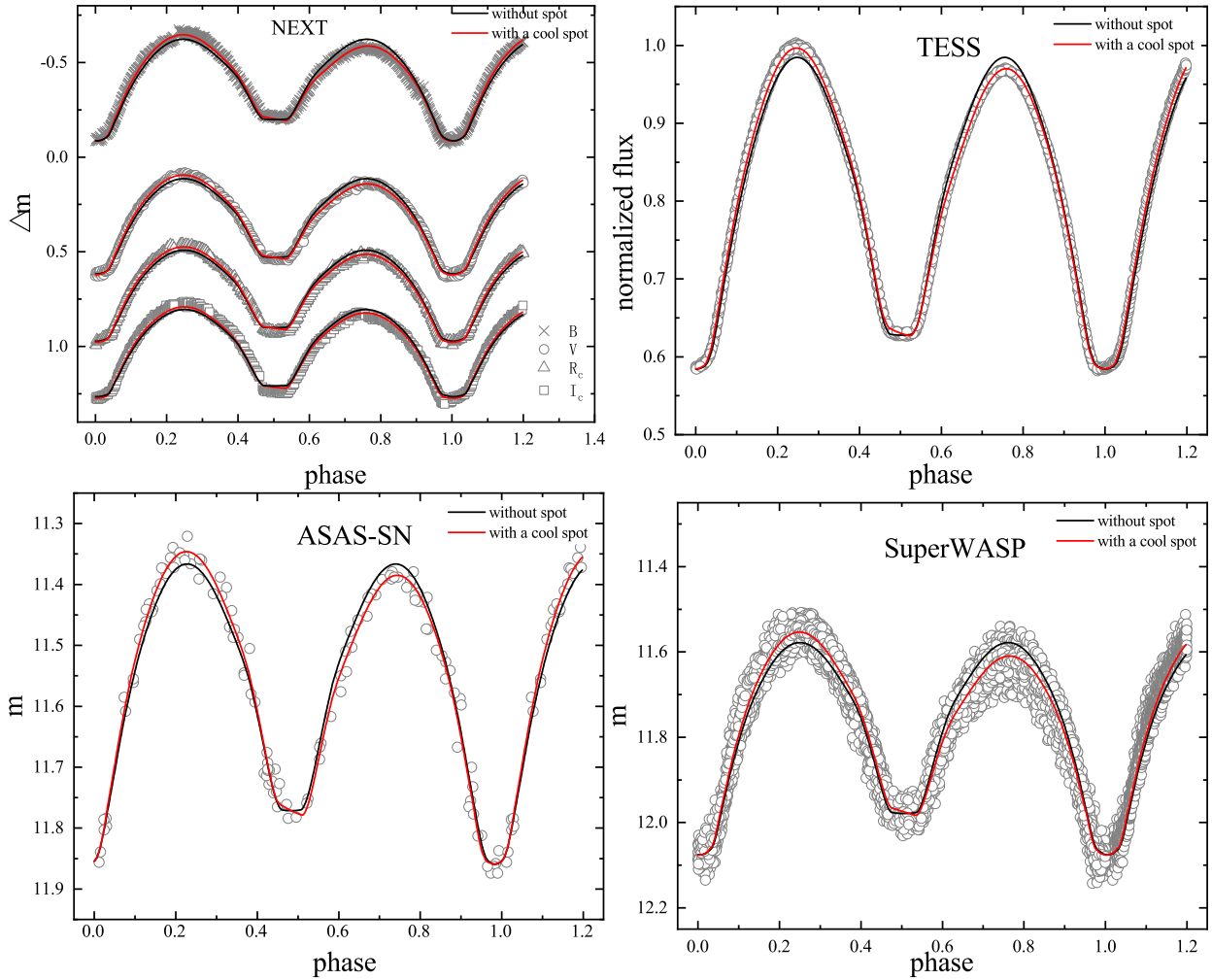


Figure 3. Theoretical and observed light curves of KN Per determined by NEXT, TESS, ASAS-SN and SuperWASP. The black lines represent the theoretical light curves without spot and the red lines represent the theoretical light of spot models.

O-C curve shows an apparently upward parabolic trend. According to the least square method, the following equation was calculated:

$$\begin{aligned} Min.I = & 2449698.11777(\pm 0.00158) + 0.866464(\pm 0.0000005) \times E \\ & + 6.07(\pm 0.36) \times 10^{-10} \times E^2. \end{aligned} \quad (4)$$

Based on the coefficient of its second order term, we calculated the rate of the increasing orbital period to be $5.12 \pm (0.30) \times 10^{-7}$ d/yr.

5. SPECTRAL ANALYSIS

The analysis of chromospheric lines was carried out with the spectral subtraction technique (Barden 1985). There are four steps in the analysis process. Firstly, we used iSpec (iSpec is a tool to treat and analyze stellar spectra) to obtain the synthesized spectrum through some input parameters (Blanco-Cuaresma et al. 2014; Blanco-Cuaresma 2019). The parameters included the effective temperature, surface gravity, metallicity, resolution and the range of wavelength. Secondly, LAMOST spectra of KN Per and the synthesized spectrum were normalized. Thirdly, we determined the wavelength of H_α (λ) of the synthesized and observed spectra, calculated their difference ($\Delta\lambda$) and obtained $\Delta\lambda/\lambda$. We shifted the synthesized spectrum based on $\Delta\lambda/\lambda$. Finally, we obtained the subtracted spectra, the difference between the observed spectra and the synthesized spectrum. Figure 6 displays the observed, synthesized and subtracted spectra. The left panel refers to data on December 25, 2012, while the right panel represents those

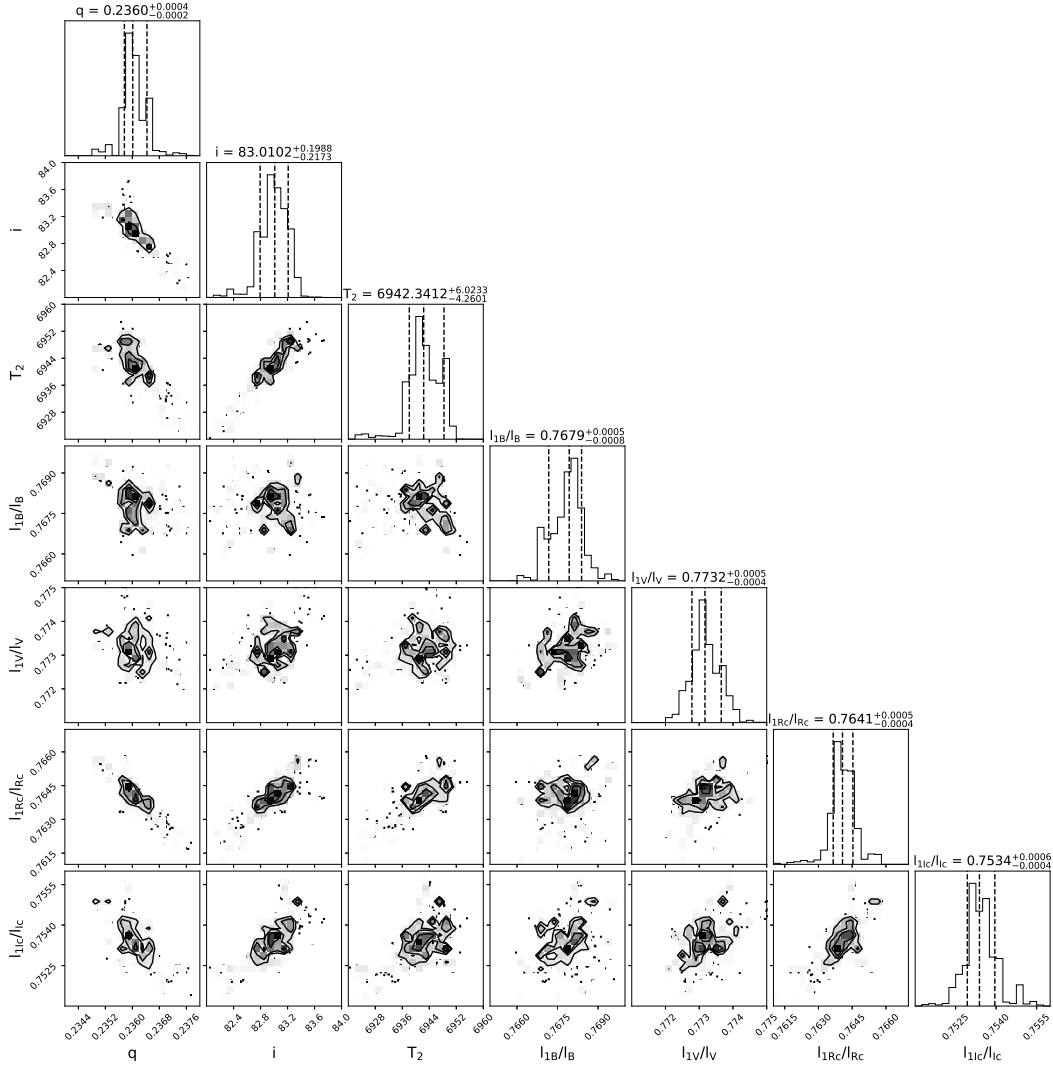


Figure 4. The probability distributions of q , i , T_2 and $L_1/(L_1 + L_2)$ determined by the MCMC modeling for the NEXT light curves.

on November 16, 2016. With Splot package of IRAF, the equivalent widths (EWs) of H_α were determined, shown in Table 4.

6. DISCUSSION AND CONCLUSION

To further investigate the structure and evolution of KN Per, the photometric and spectroscopic studies were carried out in this paper. The flat bottom near phase 0.5 indicates that KN Per is a totally eclipsing binary. Thus, the photometric solutions are reliable (Pribulla et al. 2003b; Terrell & Wilson 2005; Li et al. 2021b). Therefore, KN Per is an A-type long period DLMROB ($P=0.8664606$ days, $q=0.236$, $f=53.4\%$). A cool spot on the primary star was used to fit the observed light curves better. For the photometric analysis, the physical parameters obtained by us are similar to those from Goderya et al. (1997). For the spectroscopic analysis, the magnetic activity emission line indicator, H_α , existing in the subtracted spectra, means that KN Per has weak magnetic activity. With all available minimum times, an upward parabolic trend are displayed in the O-C diagram. The increasing rate of period is $5.12 \pm (0.30) \times 10^{-7}$ d/yr, which is due to the mass transfer from the secondary component to the primary component. The material transfer rate is calculated as $1.28 \times 10^{-7} M_\odot/\text{yr}$.

A statistic of 70 long period ($P > 0.5$ days) contact binaries containing our target is included in this paper. All collected systems were divided into two parts: the contact binaries with radial velocity observations and the contact binaries without radial velocity observations. For systems with radial velocity observations, the physical parameters

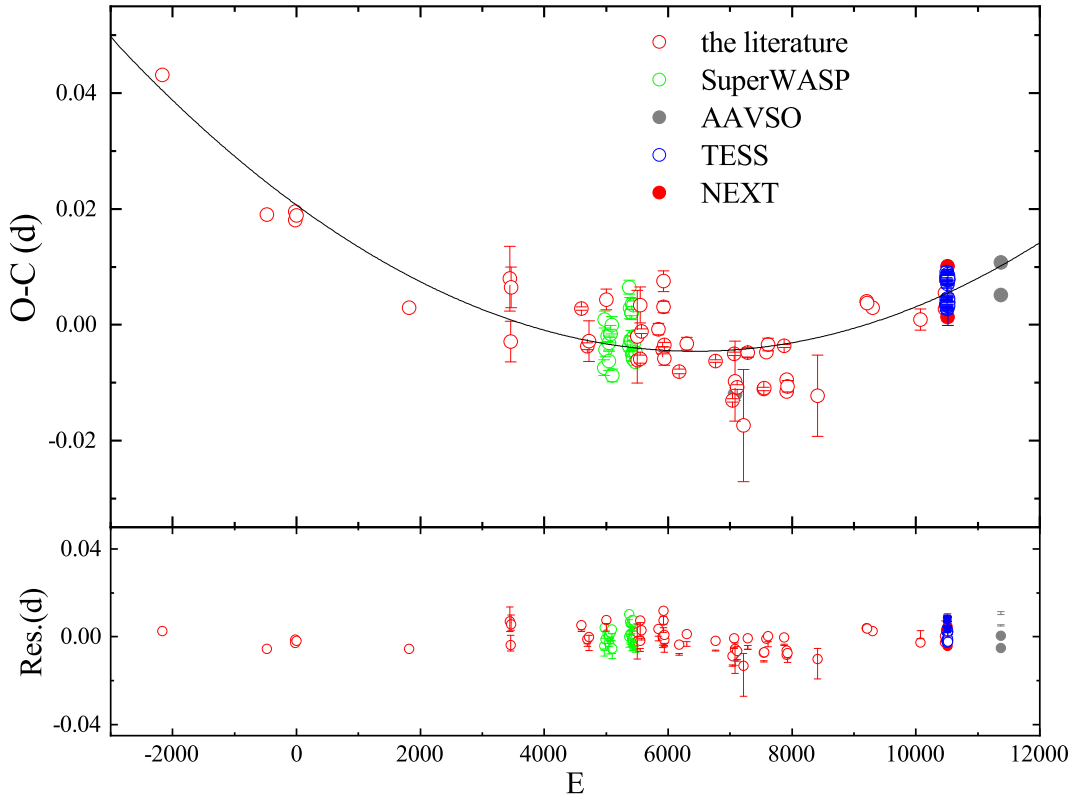


Figure 5. The upper illustration refers to O-C diagram. The lower illustration shows the residuals. The data shown in the red hollow points are from the literature, the green hollow points are from SuperWASP, the gray solid points represent data from AAVSO, the blue hollow points are samples obtained from TESS and the red solid points are from NEXT.

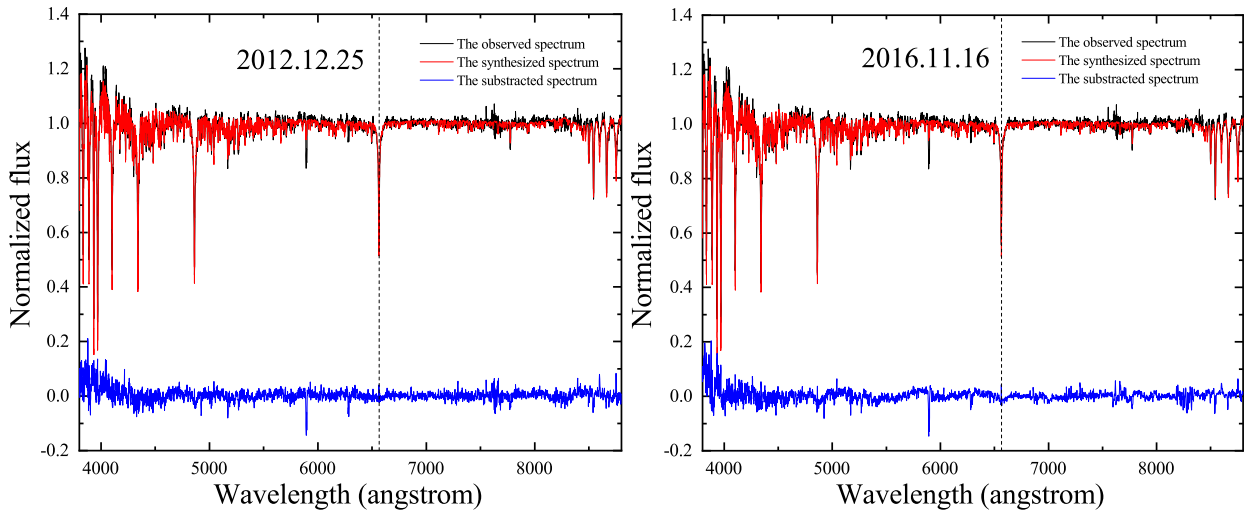


Figure 6. The normalized observed, synthesized and subtracted spectra observed by LAMOST. The left panel refers to the data on December 25, 2012, while the right panel represents those on November 16, 2016. The black lines represent the observed spectrum, the red lines represent the synthesized spectrum, and the blue lines represent the subtracted spectrum. The dotted lines represent the locations of H_{α} .

are shown in Table 7, containing the type, the brightest V-band magnitude V_{max} , period P , photometric mass ratio q_{ph} , spectroscopic mass ratio q_{sp} , relative radii r_1 and r_2 , surface temperatures T_1 and T_2 of each component, contact degree f , orbital inclination in degree i , the semimajor axis a , the absolute masses M_1 and M_2 , the absolute luminosity L_1 and L_2 , the absolute radii R_1 and R_2 , the spin angular to the orbital angular momentum ratio J_s/J_o and orbital

Table 6. The minimum timings of KN Per

BJD	Error	E	O-C	Residual	Ref.	BJD	Error	E	O-C	Residual	Ref.
2400000+						2400000+					
47820.92965	-	-2166.5	0.04312	0.00089	(1)	56007.30475	0.00080	7281.5	-0.00482	-0.00007	(18)
49283.94271	-	-478	0.01901	-0.00655	(1)	56233.88077	0.00030	7543	-0.01111	-0.00667	(22)
49679.92072	-	-21	0.01952	-0.00214	(1)	56239.07977	-	7549	-0.01094	-0.00650	(23)
49680.78572	-	-20	0.01805	-0.00360	(1)	56268.11277	-	7582.5	-0.00473	-0.00035	(23)
...
55863.89775	0.00040	7116	-0.01078	-0.00589	(21)	58813.38091	0.00069	10520	0.00328	-0.00186	(29)
55951.40475	0.00970	7217	-0.01740	-0.01260	(17)	58813.81877	0.00085	10520.5	0.00791	0.00277	(29)
56007.30475	0.00080	7281.5	-0.00482	-0.00007	(18)	59550.75006	0.00032	11371	0.00515	-0.00478	(19)
56007.30475	0.00080	7281.5	-0.00482	-0.00007	(18)	59552.92182	0.00070	11373.5	0.01074	0.00079	(19)

(1) Goderya et al. (1997); (2) <http://var.astro.cz/ocgate/>; (3) Hubscher (2005); (4) Dvorak (2006); (5) Hubscher et al. (2006); (6) Hubscher & Walter (2007); (7) SuperWASP; (8) Hubscher et al. (2009a); (9) Hubscher et al. (2008); (10) VSB; (11) Hubscher et al. (2009b); (12) Hubscher et al. (2010a); (13) Brat et al. (2009); (14) Diethelm (2009); (15) Hubscher et al. (2010b); (16) Diethelm (2011); (17) Hubscher & Lehmann (2012); (18) Hoňková et al. (2013); (19) AAVSO; (20) Hubscher (2013); (21) Diethelm (2012); (22) Diethelm (2013); (23) Corfini et al. (2014); (24) Honková et al. (2014); (25) Hubscher (2014); (26) Hubscher (2015); (27) BRNO; (28) BAVJ; (29) TESS; (30) our data.

Note. This table is available in its entirety in machine-readable form. A portion is shown here for guidance regarding its form and content.

angular momentum $\log J_o$. For contact binaries without radial velocity observations, the physical parameters shown in Table 8, are the same as Table 7. Among all collected contact binaries, 24 contact binary systems are similar to our target. They are DLMROBs with long period. Because the contact binaries displayed in Table 8 did not have the radial velocity observations, we can not calculate their absolute parameters directly. To estimate their absolute parameters, we obtained the relationship between the period (P) and the semimajor axis (a) by using 26 contact binaries with radial velocity observations. Because the period range of contact binaries without radial velocity observations collected in this paper is from 0.5 days to 1 days, we used contact binaries with period near and less than 1 days to determine the relation of P-a. A linear equation was used to fit it, which is shown as follows:

$$a = 1.02(\pm 0.32) + 4.79(\pm 0.45)P. \quad (5)$$

The relation of P-a is shown in Figure 7. The RMS of this relation is 0.68. To verify the accuracy of Equation (5), we recalculated the semimajor axis of the binaries with radial velocity observations by the Equation (5). Then, we obtained the differences between the calculated semimajor axis and the original semimajor axis. The ratios of the differences and the the semimajor axis $\Delta\alpha$ were determined. There are 74% systems with $\Delta\alpha$ less than 10%. Additionally, we calculated the semimajor axis of the binaries without radial velocity observations using the above equation. R_1 and R_2 were obtained by the relative radii and the semimajor axis. Then, according to the third law of Kepler: $M_1 (M_\odot) + M_2 = 0.0134a^3 / P^2$ and $M_2 = M_1 \times q$, the masses of the two components were determined. The units of M, a and P are M_\odot , R_\odot and d. Finally, we obtained L_1 and L_2 by $L = 4\pi\sigma T^4 R^2$. We show the absolute parameters of the binaries without radial velocity observations in Table 8, containing the semimajor axis a, the absolute masses M_1 and M_2 , the absolute luminosity L_1 and L_2 , the absolute radii R_1 and R_2 . The uncertainties of all absolute parameters of KN Per were obtained by using the error propagation, which are displayed in Table 9.

The relations of qR_2/R_1 and $q-f$ are displayed in Figure 8 and two equations were used to fit them. The range of the ratio of secondary radius to primary radius is 0.3 - 1.0. The equation showing the relation of qR_2/R_1 is displayed as follows:

$$R_2/R_1 = 0.27(\pm 0.01) + 1.26(\pm 0.09)q - 0.61(\pm 0.11)q^2. \quad (6)$$

Table 7. The long period ($P > 0.5$ days) contact binaries with radial velocity observations

Star	Type	V_{max} (mag)	P (days)	q_{ph}	q_{sp}	r_1	r_2	T_1 (K)	T_2 (K)	f (%)	i ($^\circ$)	a (R_\odot)	M_1 (M_\odot)	M_2 (M_\odot)	L_1 (L_\odot)	L_2 (L_\odot)	R_1 (R_\odot)	R_2 (R_\odot)	J_s/J_o (cgs)	$\log J_o$	Ref.
OO Aql	A	9.50	0.5068	0.843	0.846	0.4130	0.3840	6100	5926	37	87.7	3.35	1.06	0.90	2.45	1.89	1.41	1.31	0.0387	51.88	(1)
BV Eri	A	8.13	0.5077	0.253	0.297	0.5156	0.3077	6881	5737	37	74.5	2.99	1.07	0.32	4.65	0.77	1.51	0.89	0.0861	51.44	(2),(3)
XX Sex	A	9.32	0.5401	0.100	0.100	0.5940	0.2210	6881	6378	42	74.9	3.15	1.30	0.13	7.02	0.72	1.87	0.70	0.2361	51.18	(1)
V337 Peg	A	9.01	0.5785	0.401	0.401	0.5410	0.3190	7000	6438	10	73.2	3.92	1.72	0.69	9.67	2.41	2.12	1.25	0.0699	51.96	(4),(5)
V401 Cyg	A	10.53	0.5827	0.300	0.290	0.5111	0.3070	6700	6650	46	77.0	3.80	1.68	0.49	6.57	2.39	1.91	1.17	0.0753	51.83	(6),(7)
ϵ CrA	A	4.74	0.5914	0.128	0.137	0.5688	0.2290	6678	6341	25	0.7	3.69	1.70	0.23	7.75	1.02	2.10	0.85	0.1746	51.50	(8),(9)
HI Dra	A	9.02	0.5974	0.250	0.250	0.5130	0.2798	7220	6890	24	54.0	3.86	1.72	0.43	9.60	2.40	1.98	1.08	0.0848	51.78	(10),(11),(12)
V402 Aur	A	8.84	0.6035	0.201	0.201	0.5237	0.2505	6775	6700	3	0.5	3.77	1.64	0.33	7.43	1.49	2.00	0.92	0.1029	51.66	(13),(14)
RR Cen	A	7.27	0.6057	0.205	0.210	0.5353	0.2782	6912	6891	35	81.0	3.92	1.82	0.38	8.89	2.20	2.10	1.05	0.1067	51.74	(15)
BX AND	A	9.05	0.6101	0.623	0.445	0.4500	0.3200	6650	4758	5	75.9	4.42	2.15	0.98	7.08	0.90	2.01	1.40	0.0416	52.22	(16)
UZ Leo	A	9.61	0.6180	0.233	0.303	0.5140	0.3130	6980	6772	76	87.4	4.21	2.01	0.82	10.60	3.68	2.23	1.40	0.0911	51.91	(17)
SZ Hor	A	11.01	0.6251	0.470	0.473	0.4550	0.3230	6881	6169	18	80.4	4.38	1.82	0.86	7.61	1.23	1.95	1.38	0.0481	52.08	(2)
V535 Ara	A	7.17	0.6293	0.361	0.302	0.4976	0.2921	8200	8129	22	79.9	4.20	1.94	0.59	18.00	6.00	2.09	1.23	0.0630	51.99	(18)
V407 Peg	A	9.70	0.6369	0.256	0.256	0.4700	0.3120	6980	6484	81	71.1	4.02	1.72	0.43	9.80	2.33	2.15	1.21	0.0724	51.79	(4),(17)
V868 Mon	A	8.90	0.6377	0.373	0.373	0.4960	0.3290	7000	6584	49	72.1	4.45	2.39	0.89	14.70	3.89	2.33	1.56	0.0633	52.18	(10)
FP Boo	A	10.14	0.6405	0.100	0.096	0.5944	0.2147	6980	6456	38	68.8	3.78	1.61	0.15	11.19	0.92	2.31	0.77	0.2362	51.36	(19),(20)
AG Vir	A	8.50	0.6427	0.382	0.382	0.4890	0.3240	8150	6953	17	84.4	4.48	2.18	0.74	19.00	3.85	2.19	1.36	0.0606	52.11	(21)
FN Cam	W	8.58	0.6771	0.222	0.222	0.5569	0.3178	6700	6848	88	71.2	4.65	2.40	0.53	12.11	4.32	2.59	1.48	0.1098	51.99	(22)
V1073 Cyg	A	8.52	0.7859	0.319	0.303	0.4920	0.2863	7300	6609	12	68.4	5.17	1.81	0.55	16.48	3.75	2.55	1.48	0.0665	51.94	(23)
MW Pav	W	8.51	0.7950	0.222	0.228	0.5428	0.2894	6900	6969	60	86.4	4.43	1.51	0.33	11.82	3.31	2.41	1.28	0.1034	51.67	(24)
V376 And	A	7.02	0.7987	0.305	0.305	0.4890	0.2850	9000	7080	7	62.7	5.32	2.44	0.74	40.00	5.00	2.60	1.51	0.0677	52.15	(24)
V2388 Oph	A	8.48	0.8023	0.186	0.186	0.5553	0.2781	6900	6349	65	74.7	4.68	1.80	0.34	13.50	2.43	2.60	1.30	0.1235	51.73	(25)
TY Pup	W	8.62	0.8192	0.184	0.246	0.5170	0.3130	6900	6915	84	83.6	4.65	1.65	0.30	14.11	3.86	2.64	1.37	0.1102	51.67	(2),(26)
II Uma	W	8.17	0.8252	0.172	0.186	0.5682	0.2828	6550	6554	87	77.8	4.87	1.94	0.33	12.14	2.62	2.73	1.32	0.1376	51.76	(27)
V921 Her	A	9.44	0.8774	0.227	0.226	0.5113	0.2577	7780	7346	23	68.1	5.29	2.07	0.51	5.09	5.60	1.41	0.25	0.0898	51.94	(20),(28)
DU Boo	A	8.59	1.0559	0.199	0.206	0.5343	0.2915	7850	7610	50	81.0	5.97	2.08	0.49	33.42	6.32	3.19	1.74	0.1093	51.92	(29),(30)
TU Mus	A	8.25	1.3870	0.652	0.678	0.4500	0.3700	38700	33200	5	77.8	17.70	16.70	10.40	104712	35481	7.20	5.70	0.0444	53.91	(31)
V606 Cen	A	9.35	1.4951	0.541	0.527	0.4358	0.3281	29200	21770	4	87.3	15.58	14.70	7.96	30400	5440	6.83	5.19	0.0424	53.77	(32)
V382 cyg	A	8.33	1.8855	0.677	0.742	0.4139	0.3604	36000	34415	9	84.5	23.45	27.90	20.80	141905	89949	9.70	8.50	0.0385	54.38	(33)
LY Aur	W	6.68	4.0020	0.528	0.528	0.4480	0.3510	31000	31150	-	87.9	36.10	25.50	14.00	213796	134896	16.10	12.60	0.0461	54.31	(34),(35)

(1) Pribulla et al. (2007); (2) Duerbeck & Rucinski (2007); (3) Deb & Singh (2011); (4) Rucinski et al. (2008); (5) Ekmekci et al. (2012); (6) Rucinski et al. (2002); (7) Wolf et al. (2000); (8) Yang et al. (2005b); (9) Goeking & Duerbeck (1993); (10) Pribulla et al. (2009); (11) Caliskan et al. (2014); (12) Papanicolaou & Christopoulos (2015); (13) Zola et al. (2004); (14) Pych et al. (2004); (15) Yang et al. (2005b); (16) Partovi et al. (2021); (17) Lee & Park (2018); (18) Ozkardes & Erdem (2012); (19) Rucinski et al. (2005); (20) Gazess et al. (2006); (21) Pribulla et al. (2006); (22) Rucinski et al. (2001); (23) Rucinski et al. (2002); (24) Cizek (2011); (25) Yokut et al. (2004); (26) Sarosakulchai et al. (2018); (27) Zhou et al. (2016); (28) Rucinski et al. (2003); (29) Djurašević et al. (2013); (30) Pribulla et al. (2011); (31) Terrell et al. (2003); (32) Li et al. (2022); (33) Yaşarsay & Yokut (2013); (34) Zhao et al. (2014); (35) Stieckland et al. (1994)

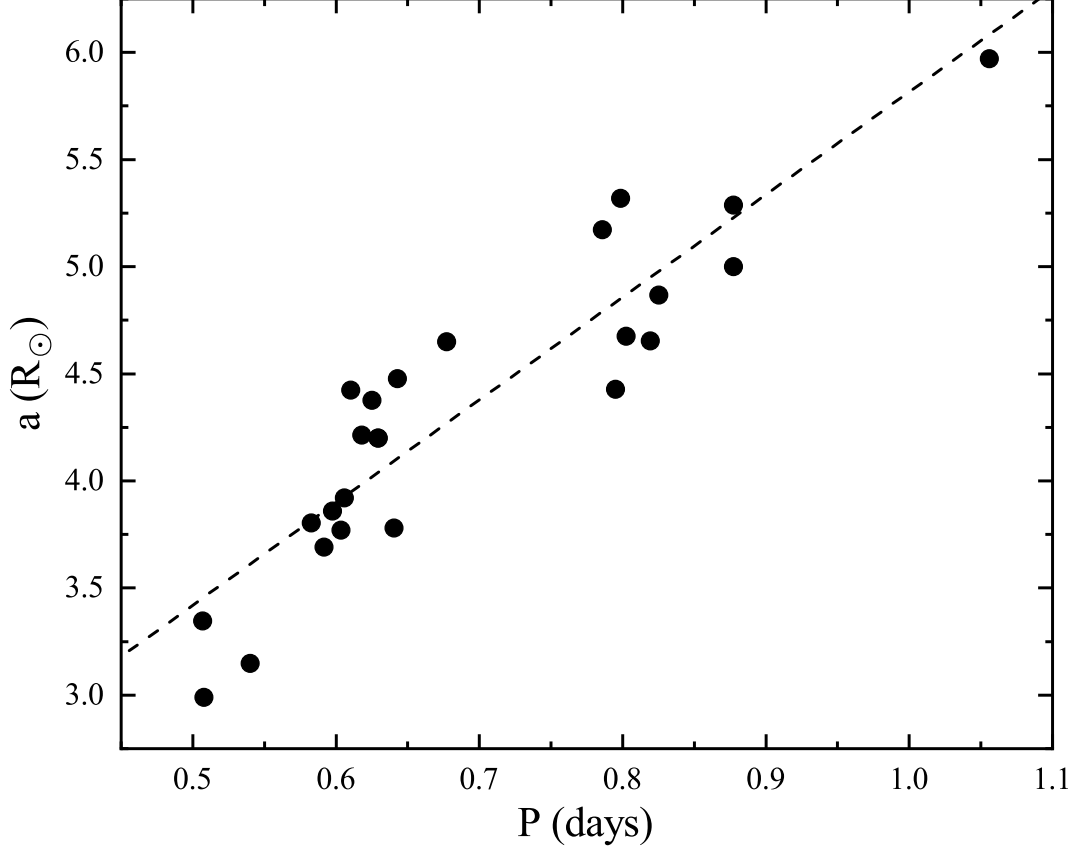
Table 8. The long period ($P > 0.5$ days) contact binaries without radial velocity observations

Star	Type	V_{max} (mag)	P (days)	q_{ph}	r_1	r_2	T_1 (K)	T_2 (K)	f (%)	i ($^\circ$)	a (R_\odot)	M_1 (M_\odot)	M_2 (M_\odot)	L_1 (L_\odot)	L_2 (L_\odot)	R_1 (R_\odot)	R_2 (R_\odot)	J_s/J_o	$\log J_o$ (cgs)	Ref.
CSS J161753.6+205014	A	14.60	0.5098	0.080	0.5980	0.1930	7006	6864	4	78.0	6.14	1.99	0.16	9.28	0.89	2.07	0.67	0.2921	51.39	(1)
BU Vel	A	10.48	0.5163	0.251	0.5065	0.2999	7500	7448	61	84.9	10.55	1.72	0.43	8.90	3.03	1.77	1.05	0.0835	51.76	(2)
VV Cet	A	10.54	0.5224	0.249	0.5100	0.2600	8100	5900	16	80.2	3.53	1.72	0.43	12.48	0.91	1.80	0.92	0.0833	51.76	(3)
NSVS 13602901	A	12.03	0.5238	0.171	0.5540	0.2600	6250	6222	44	83.6	9.29	1.84	0.31	5.24	1.13	1.96	0.92	0.1309	51.65	(4)
CSS J145437.2+060239	A	15.28	0.5437	0.110	0.5860	0.2270	6930	6336	43	79.3	7.26	1.95	0.21	9.34	0.98	2.13	0.82	0.2113	51.52	(1)
KIC 8145477	A	14.66	0.5658	0.099	0.6030	0.2321	6538	6284	76	84.4	10.38	1.98	0.20	8.30	1.05	2.25	0.87	0.2462	51.49	(5)
AP Aur	A	11.13	0.5694	0.246	0.5238	0.2843	9016	8703	64	75.9	10.53	1.75	0.43	22.87	5.85	1.97	1.07	0.0894	51.78	(6)
CSS J021552.4+324419	A	14.68	0.5738	0.110	0.5800	0.2210	6863	6315	25	79.3	9.42	1.97	0.22	9.52	0.99	2.19	0.83	0.2069	51.53	(1)
CSS J210300.1+050345	A	13.90	0.5922	0.100	0.5900	0.2170	6787	6188	34	82.8	9.17	2.00	0.20	9.87	0.92	2.28	0.84	0.2329	51.51	(1)
CSS J211420.2-142710	A	15.32	0.5981	0.110	0.5780	0.2180	6876	6171	18	74.3	9.27	1.99	0.22	10.12	0.93	2.25	0.85	0.2054	51.54	(1)
CSS J234145.7+233158	A	13.91	0.5986	0.090	0.6100	0.2260	6853	6852	78	77.7	10.54	2.02	0.18	11.14	1.53	2.37	0.88	0.2737	51.47	(1)
KIC 7601767	A	14.46	0.5992	0.161	0.5507	0.2464	6567	6388	23	77.4	3.89	1.90	0.31	7.67	1.37	2.14	0.96	0.1354	51.56	(5)
KIC 7698650	A	14.98	0.5992	0.116	0.5923	0.2439	6307	6261	74	81.8	10.72	1.98	0.23	7.54	1.24	2.31	0.95	0.2063	51.67	(5)
NX Cam	A	10.70	0.6058	0.150	0.5639	0.2548	6657	6015	55	82.4	9.74	1.92	0.29	8.62	1.17	2.21	1.00	0.1508	51.65	(7)
KIC 8554005	W	12.79	0.6083	0.356	0.5100	0.3345	7298	7302	59	83.3	10.23	1.63	0.58	10.26	4.42	2.01	1.32	0.0686	51.88	(5)
EK Aqr	A	11.01	0.6128	0.192	0.5399	0.2632	7900	6808	33	76.4	3.96	1.86	0.36	15.95	2.09	2.14	1.04	0.1135	52.43	(8)
DN Aur	W	13.00	0.6169	0.205	0.5414	0.2765	6830	6750	54	76.9	11.32	1.84	0.38	9.05	2.25	2.15	1.10	0.1089	51.75	(9)
KIC 5290305	A	14.05	0.6210	0.210	0.5380	0.2755	6542	6186	41	81.6	10.66	1.84	0.39	7.60	1.59	2.15	1.10	0.1057	51.76	(5)
KIC 10229723	A	12.04	0.6287	0.141	0.5681	0.2457	6477	6262	44	81.5	9.76	1.95	0.28	8.29	1.35	2.29	0.99	0.1606	51.64	(5)
CSS J234324.8+211100	A	14.50	0.6311	0.110	0.5940	0.2370	6640	6603	68	80.6	10.32	2.01	0.22	10.07	1.57	2.40	0.96	0.2174	51.56	(1)
KIC 11144556	A	13.43	0.6430	0.160	0.5824	0.2847	6803	6702	100	76.7	11.47	1.93	0.31	10.97	2.47	2.39	1.17	0.1532	51.69	(5)
KIC 10007533	A	13.74	0.6481	0.082	0.6061	0.2800	6977	6379	44	83.4	10.28	2.07	0.17	13.30	1.09	2.50	0.86	0.2923	51.46	(5)
KIC 3127873	A	15.49	0.6715	0.109	0.6042	0.2495	6408	6164	98	87.5	10.97	2.04	0.22	9.92	1.45	2.56	1.06	0.2274	51.58	(5)
IK Per	A	11.15	0.6760	0.191	0.5482	0.2724	9070	7470	52	77.8	10.82	1.91	0.36	33.11	3.76	2.34	1.16	0.1177	51.76	(10)
KIC 11618883	W	12.44	0.6849	0.225	0.5523	0.3045	4347	4403	80	87.6	12.52	1.86	0.42	1.81	0.58	2.38	1.31	0.1064	51.81	(5)
KIC 9453192	A	13.89	0.7188	0.140	0.5754	0.2524	6622	6161	61	85.1	9.94	2.03	0.28	11.39	1.64	2.57	1.13	0.1666	51.68	(5)
KIC 12352712	A	16.41	0.7221	0.095	0.6088	0.2338	6667	6469	87	89.4	10.75	2.12	0.20	13.19	1.72	2.73	1.05	0.2594	51.55	(5)
KIC 9350889	W	13.44	0.7259	0.148	0.5827	0.2720	6996	7035	90	87.4	11.16	2.02	0.30	14.77	3.29	2.62	1.22	0.1628	51.71	(5)
CSS J030702.2+261521	A	13.98	0.7284	0.090	0.5990	0.2130	6680	6362	42	81.2	10.71	2.13	0.19	13.04	1.36	2.70	0.96	0.2637	51.54	(1)
KIC 8539720	A	12.93	0.7445	0.148	0.5828	0.2717	6658	6398	90	82.5	11.24	2.04	0.30	12.60	2.34	2.68	1.25	0.1632	51.72	(5)
CSS J051156.6+011756	A	14.82	0.7527	0.150	0.5600	0.2450	6414	5936	32	83.1	10.79	2.04	0.31	10.20	1.43	2.59	1.13	0.1484	51.72	(1)
CSS J022044.4+280006	A	14.42	0.7594	0.150	0.5630	0.2490	6760	6382	41	84.7	10.81	2.05	0.31	12.89	2.00	2.62	1.16	0.1501	51.73	(1)
KIC 8265951	A	12.34	0.7800	0.155	0.5601	0.2509	6943	6648	53	79.7	8.36	2.06	0.32	14.80	2.50	2.67	1.19	0.1449	51.75	(5)
KIC 5439790	A	13.19	0.7961	0.197	0.5415	0.2691	7022	6804	39	83.0	8.28	2.00	0.39	14.95	3.26	2.62	1.30	0.1121	51.83	(5)
V343 Ori	W	10.76	0.8091	0.253	0.5496	0.3313	7150	7312	87	79.7	9.65	1.92	0.49	16.99	6.75	2.69	1.62	0.0980	51.91	(11)
V2787 Ori	A	12.70	0.8110	0.120	0.5717	0.2225	6993	5418	18	84.7	10.24	2.15	0.26	16.88	3.92	2.81	1.09	0.1863	51.68	(12)
KIC 3104113	W	11.50	0.8468	0.171	0.5777	0.2897	6535	6640	98	79.5	5.08	2.09	0.36	14.08	3.77	2.94	1.45	0.1430	51.81	(5)
KN Per	A	11.52	0.8665	0.236	0.5712	0.3045	7200	7156	68	85.97	5.18	1.99	0.49	13.54	2.43	2.85	1.28	0.9710	51.93	(13)
NS Cam	A	12.78	0.9074	0.213	0.5242	0.2619	6250	5689	17	85.0	9.57	2.08	0.44	10.84	1.86	2.82	1.41	0.0989	51.91	(14)
KIC 11097678	A	13.25	0.9997	0.095	0.6103	0.2348	6493	6427	91	83.4	10.99	2.41	0.23	20.05	2.85	3.55	1.37	0.2625	51.69	(5)

(1) Christopoulou et al. (2022a); (2) Twigg (1979); (3) Rahman (2000); (4) Wadhwa et al. (2021b); (5) Dobski (2021); (6) Li et al. (2001); (7) Martignoni et al. (2021); (8) Gao et al. (2022); (9) Coderya et al. (1996); (10) Zhu et al. (2005); (11) Yıldırım & Soydogan (2017); (12) Tian et al. (2019); (13) this paper; (14) Samec et al. (2020)

Table 9. The uncertainties of the absolute parameters of KN Per

a	M ₁	M ₂	L ₁	L ₂	R ₁	R ₂
(R _⊙)	(M _⊙)	(M _⊙)	(L _⊙)	(L _⊙)	(R _⊙)	(R _⊙)
0.71	0.83	0.20	0.41	0.22	2.40	0.58

**Figure 7.** The relationship between the period (P) and the semimajor axis (a).

From the left panel of Figure 8, barely binary systems are deviated from the general tendency of this equation. From the right panel of Figure 8, the locations of the contact binaries with small mass ratio ($q \leq 0.3$) are distributed and the contact degree of them are from 0 % to 100 % and the contact degree of the systems with mass ratio more than 0.3 are smaller than 70 % and decrease with the increasing mass ratio. A nonlinear equation was applied to fit it,

$$f = 25.56(\pm 28.82) + 41.94(\pm 21.31)e^{-2.96(\pm 1.76)q}. \quad (7)$$

Christopoulou et al. (2022b) found that the smallest the q value, the larger the contact degree distribution range. Our result is similar to the study of them.

With $k_{1,2}^2$ fixed on 0.06 (Li & Zhang 2006), the ratios of the spin angular momentum to the orbital angular momentum (J_s/J_o) were calculated by the following equation from Yang & Qian (2015):

$$\frac{J_s}{J_o} = \frac{1+q}{q} [(k_1 r_1)^2 + (k_2 r_2)^2 q], \quad (8)$$

where $r_{1,2}$ refer to the relative radii and $k_{1,2}^2$ are the dimensionless gyration radii. We display the relation of q - J_s/J_o of all collected systems in Figure 9 and the dashed line is the boundary to distinguish stable boundary and unstable boundary. It was obvious that the value of J_s/J_o falls with the increasing mass ratio. We used an exponential equation to fit it:

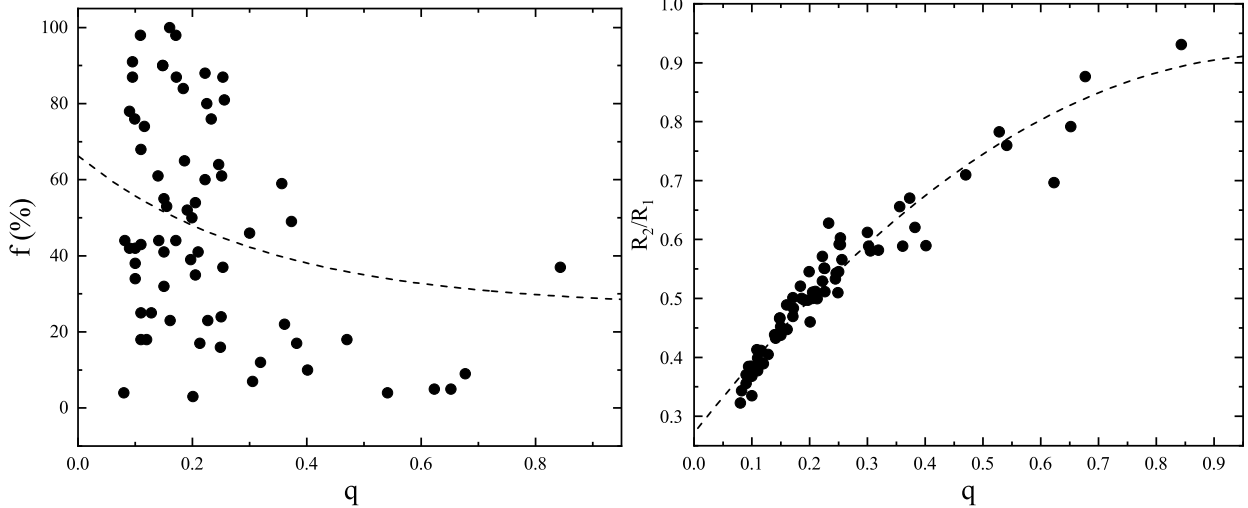


Figure 8. The relations of q - R_2/R_1 (left) and q - f (right).

$$\frac{J_s}{J_o} = 0.050(\pm 0.002) + 0.602(\pm 0.019) \times e^{-11.581(\pm 0.353) \times q}. \quad (9)$$

The predicted minimum is the mass ratio corresponding to $J_s/J_o=1/3$. A predicted minimum mass ratio was calculated as 0.0652. The minimum mass ratio was determined as $q_{min} \sim 0.076$ when considering the rotation of the secondary component and the dimensionless gyration radii $k_1^2 = k_2^2 = 0.06$ (Li & Zhang 2006). The value was derived as 0.070 \sim 0.074 when considering the rotation effect (Arbutina 2007, 2009). A predicted minimum mass ratio was calculated as 0.0652. Our result is consistent with many previous studies (Li & Zhang 2006; Li et al. 2021a).

We divided all collected contact binaries into two types: A-type and W-type. With the parameters displayed in Table 7 and Table 8, the relations of mass-radius (M-R) and mass-luminosity (M-L) are shown in Figure 10. According to Hurley et al. (2002), the zero-age main-sequence (ZAMS) and the terminal-age main-sequence (TAMS) are determined from the binaries evolution code, which are displayed as the solid and dashed lines in Figure 10. We use the circles to represent the two components of A-type contact binaries, the triangles to refer to the two components of W-type contact binaries, and the two red circles to represent the two components of KN Per. The open symbols refer to the more massive stars of A-type contact binaries and the solid symbols refer to the less massive stars of A-type binaries. For W-type contact binaries, The open symbols and the solid symbols also refer to the more massive stars and the less massive stars, respectively. The locations of the two components in KN Per are in accord with those of other stars. For both A-type contact binaries and W-type contact binaries, most of the primary components are situated between the lines of "ZAMS" and "TAMS", signifying that they are main sequence stars. While most of the secondary components of both A-type contact binaries and W-type contact binaries are situated above the line of "TAMS", implying that they have evolved from the main sequence stage. Contrast to the secondary components, the primary components are located near the line of "ZAMS". It indicates that the evolutionary stages of the primary components are earlier than those of the secondary components, the reason of which may be the energy and mass transfer from the primary components to the secondary components. The result obtained by us supports the result obtained by previous researchers (Yakut & Eggleton 2005; Qian et al. 2017, 2018).

With the total mass of the binary M_T (solar unit), P (days) and q , we calculated the orbital angular momentum J_o of the collected contact binaries, based on the following equation from Christopoulou & Papageorgiou (2013):

$$J_o = 1.24 \times 10^{52} \times M_T^{3/5} \times P^{1/3} \times q \times (1 + q)^{-2}. \quad (10)$$

The relation of $\log M_T - \log J_o$ is shown in Figure 11, containing the detached binary systems and the boundary line. The boundary segregates detached and contact binaries (Eker et al. 2006). Nearly all contact binary systems are located below the boundary, while the detached binaries are situated above it. This means that J_o of contact binary systems are less than those of detached binary systems with the same mass. This is due to the angular momentum loss while contact binaries were forming and evolving. To some extent, this shows that the formation of DLMROBs is

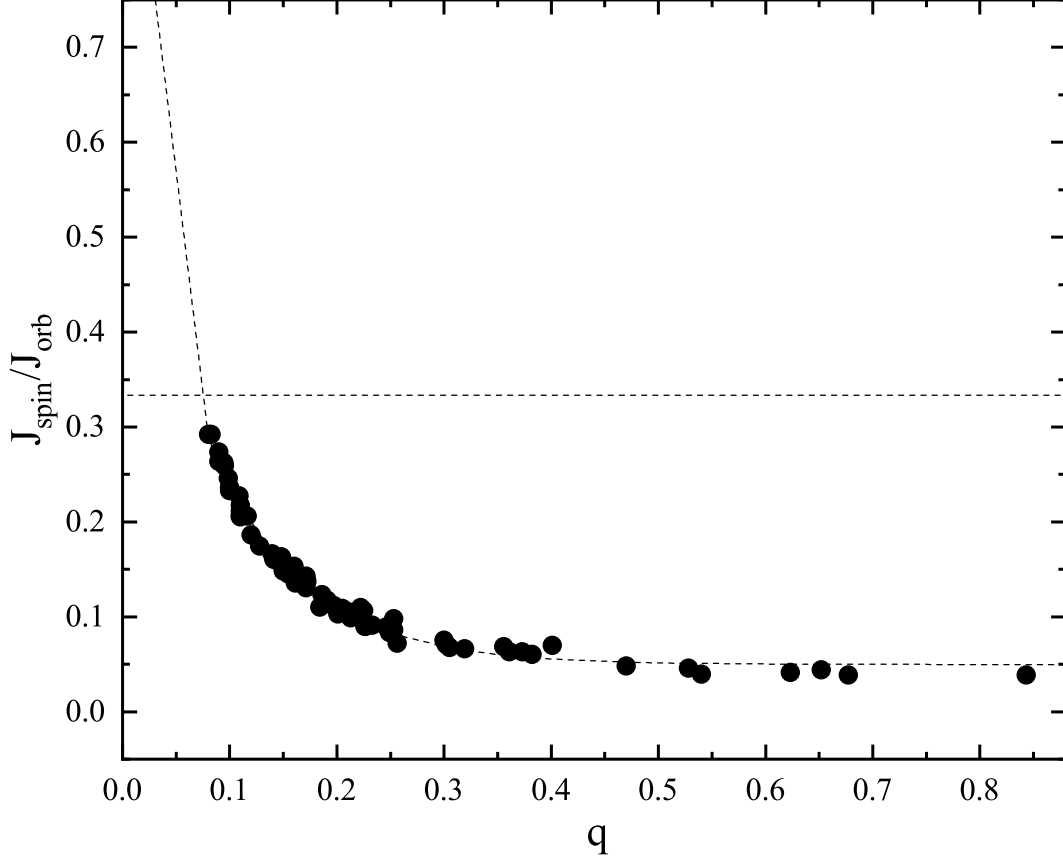


Figure 9. The q - J_s/J_o diagram, where the dashed line refers to the boundary distinguishing stable boundary and unstable boundary.

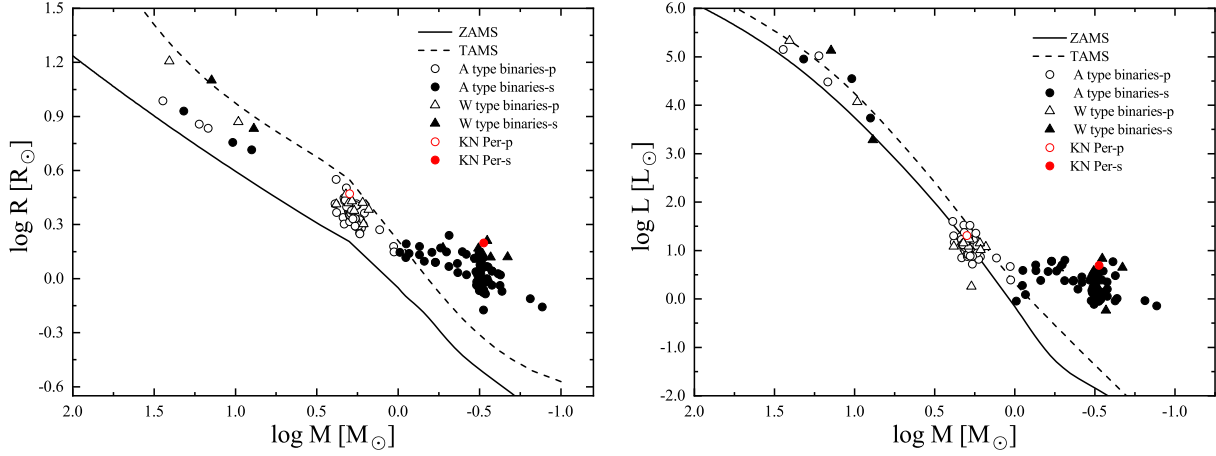


Figure 10. The mass-radius diagram (left) and the mass-luminosity diagram (right). The hollow and solid circles represent the A-type contact binaries, the open and solid triangles represent the W-type contact binaries, and the two red circles are two components of KN Per.

initially from the detached binary systems with short periods and DLMROBs are formed through angular momentum loss via magnetic stellar wind (Qian et al. 2007, 2013, 2015, 2018; Li et al. 2019).

To further explore the stability of KN Per, the instability parameters were calculated through the equations provided by Wadhwa et al. (2021a). Firstly, based on the mass of the primary component and the contact degree, we obtained the instability mass ratio q_{inst} as 0.0428. Then, with the photometric mass ratio, the contact degree and the semimajor

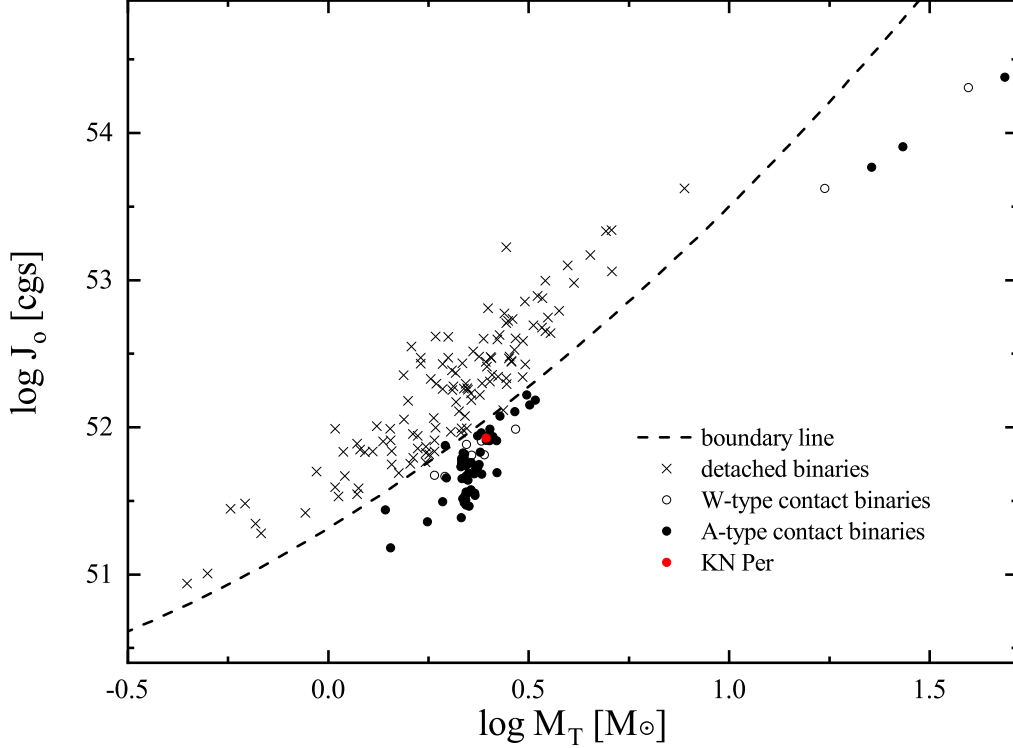


Figure 11. The relationship between orbital angular momentum and total mass for binary systems. The black crosses represent the detached binaries. The hollow circles represent the A-type contact binaries and the solid circles refer to the W-type contact binaries. KN Per is shown as the red circle.

axis, the theoretical fractional radius of the primary component was calculated, which is $2.815 R_{\odot}$. We determined the dimensionless gyration radius of the primary component ($k_1 = 0.1801$) for KN Per ($M_1 = 2.0 M_{\odot}$) from Landin et al. (2009). The value of k_2 was also obtained from this literature. With R_1 , k_1 , k_2 ($k_2^2=0.205$) and q , we determined that the instability separation A_{inst} is $3.1042 R_{\odot}$. Finally, the instability period was obtained to be 0.4025 days, according to the third law of Kepler. Because the values of q_{inst} , A_{inst} and P_{inst} are far less than the three corresponding actual parameters, KN Per is in a stable stage.

We calculated the material transfer rate using the following equation,

$$\frac{dM_1}{dt} = \frac{M_1 M_2}{3P(M_1 - M_2)} \times \frac{dP}{dt}. \quad (11)$$

The rate is $1.28 \times 10^{-7} M_{\odot}/\text{yr}$. For KN Per, the rate of period variation and mass transfer is typical for W UMa systems. The rate of period variation and mass transfer of five contact binaries are displayed in Table 10. The value is positive, showing the mass transfer from the secondary component to the primary component. It will lead to a falling mass ratio. In the future, the mass ratio of KN Per may reach the dynamic stability limit and KN Per may merge into a fast rotating star.

In conclusion, KN Per is an A-type long period DLMROB and has weak chromosphere activity due to the photometric and spectroscopic analysis. Its orbital period exhibits a continuous increase with a rate of $5.12 \pm (0.30) \times 10^{-7} \text{ d/yr}$. We also found that KN Per is in a stable stage by calculating the instability parameters and shows a mass transfer from the secondary component to the primary component.

Table 10. The rate of period variation and mass transfer of five contact binaries

Name	The rate of period variation (d yr ⁻¹)	The rate of the mass transfer (M _⊙ yr ⁻¹)	Ref.
V410 Aur	8.22×10^{-7}	1.62×10^{-7}	(1)
XY Boo	6.25×10^{-7}	1.17×10^{-7}	(1)
V1191 Cyg	4.50×10^{-7}	7.45×10^{-8}	(2)
TY Pup	5.57×10^{-8}	8.41×10^{-9}	(3)
FN Cam	4.38×10^{-7}	1.47×10^{-7}	(4)

(1) Yang et al. (2005a); (2) Zhu et al. (2011); (3) Sarotsakulchai et al. (2018); (4) Hu et al. (2018)

ACKNOWLEDGMENTS

This work is supported by the Joint Research Fund in Astronomy (No. U1931103) under cooperative agreement between National Natural Science Foundation of China (NSFC) and Chinese Academy of Sciences (CAS), and by NSFC (No. 1227301811703016), and by the Natural Science Foundation of Shandong Province (No. ZR2014AQ019), and by Young Scholars Program of Shandong University, Weihai (No. 20820171006), and by the Open Research Program of Key Laboratory for the Structure and Evolution of Celestial Objects (No. OP201704), and by the Cultivation Project for LAMOST Scientific Payoff and Research Achievement of CAMS-CAS.

This work is partly supported by the Supercomputing Center of Shandong University, Weihai.

We acknowledge the support of the staff of NEXT.

This work includes data collected by the TESS mission. Funding for the TESS mission is provided by NASA Science Mission directorate. We acknowledge the TESS team for its support of this work.

This publication makes use of data products from the AAVSO Photometric All Sky Survey (APASS). Funded by the Robert Martin Ayers Sciences Fund and the National Science Foundation.

We thank Las Cumbres Observatory and its staff for their continued support of ASAS-SN. ASAS-SN is funded in part by the Gordon and Betty Moore Foundation through grants GBMF5490 and GBMF10501 to the Ohio State University, and also funded in part by the Alfred P. Sloan Foundation grant G-2021-14192.

The spectral data were provided by Guoshoujing Telescope (the Large Sky Area Multi-Object Fiber Spectroscopic Telescope LAMOST) is a National Major Scientific Project built by the Chinese Academy of Sciences. Funding for the project has been provided by the National Development and Reform Commission. LAMOST is operated and managed by the National Astronomical Observatories, Chinese Academy of Sciences.

This paper makes use of data from the DR1 of the WASP data (Butters et al. 2010) as provided by the WASP consortium, and the computing and storage facilities at the CERIT Scientific Cloud, reg. no. CZ.1.05/3.2.00/08.0144 which is operated by Masaryk University, Czech Republic.

REFERENCES

- Antonello, E., & Mantegazza, L. 1997, *A&A*, 327, 240
- Arbutina, B. 2007, *MNRAS*, 377, 1635,
doi: [10.1111/j.1365-2966.2007.11723.x](https://doi.org/10.1111/j.1365-2966.2007.11723.x)
- . 2009, *MNRAS*, 394, 501,
doi: [10.1111/j.1365-2966.2008.14332.x](https://doi.org/10.1111/j.1365-2966.2008.14332.x)
- Barden, S. C. 1985, *ApJ*, 295, 162, doi: [10.1086/163361](https://doi.org/10.1086/163361)
- Binnendijk, L. 1970, *Vistas in Astronomy*, 12, 217,
doi: [10.1016/0083-6656\(70\)90041-3](https://doi.org/10.1016/0083-6656(70)90041-3)
- Blanco-Cuaresma, S. 2019, *MNRAS*, 486, 2075,
doi: [10.1093/mnras/stz549](https://doi.org/10.1093/mnras/stz549)
- Blanco-Cuaresma, S., Soubiran, C., Heiter, U., & Jofré, P. 2014, *A&A*, 569, A111,
doi: [10.1051/0004-6361/201423945](https://doi.org/10.1051/0004-6361/201423945)
- Brat, L., Trnka, J., Lehky, M., et al. 2009, *Open European Journal on Variable Stars*, 107, 1
- Butters, O. W., West, R. G., Anderson, D. R., et al. 2010, *A&A*, 520, L10, doi: [10.1051/0004-6361/201015655](https://doi.org/10.1051/0004-6361/201015655)
- Çalışkan, Ş., Latković, O., Djurašević, G., et al. 2014, *AJ*, 148, 126, doi: [10.1088/0004-6256/148/6/126](https://doi.org/10.1088/0004-6256/148/6/126)

- Çiçek, C. 2011, *NewA*, 16, 12,
doi: [10.1016/j.newast.2010.06.005](https://doi.org/10.1016/j.newast.2010.06.005)
- Christopoulou, P.-E., Lalounta, E., Papageorgiou, A., et al. 2022a, *MNRAS*, doi: [10.1093/mnras/stac534](https://doi.org/10.1093/mnras/stac534)
- . 2022b, *MNRAS*, 512, 1244, doi: [10.1093/mnras/stac534](https://doi.org/10.1093/mnras/stac534)
- Christopoulou, P. E., & Papageorgiou, A. 2013, *AJ*, 146, 157, doi: [10.1088/0004-6256/146/6/157](https://doi.org/10.1088/0004-6256/146/6/157)
- Conroy, K. E., Kochoska, A., Hey, D., et al. 2020, *ApJS*, 250, 34, doi: [10.3847/1538-4365/abb4e2](https://doi.org/10.3847/1538-4365/abb4e2)
- Corfini, G., Aceti, P., Arena, C., et al. 2014, *Information Bulletin on Variable Stars*, 6094, 1
- Cui, X.-Q., Zhao, Y.-H., Chu, Y.-Q., et al. 2012, *Research in Astronomy and Astrophysics*, 12, 1197, doi: [10.1088/1674-4527/12/9/003](https://doi.org/10.1088/1674-4527/12/9/003)
- Cutri, R. M., Skrutskie, M. F., van Dyk, S., et al. 2003, *VizieR Online Data Catalog*, II/246
- Deb, S., & Singh, H. P. 2011, *MNRAS*, 412, 1787, doi: [10.1111/j.1365-2966.2010.18016.x](https://doi.org/10.1111/j.1365-2966.2010.18016.x)
- Debski, B. 2021, arXiv e-prints, arXiv:2112.14823. <https://arxiv.org/abs/2112.14823>
- Diethelm, R. 2009, *Information Bulletin on Variable Stars*, 5871, 1
- . 2011, *Information Bulletin on Variable Stars*, 5960, 1
- . 2012, *Information Bulletin on Variable Stars*, 6011, 1
- . 2013, *Information Bulletin on Variable Stars*, 6042, 1
- Djurašević, G., Baştürk, Ö., Latković, O., et al. 2013, *AJ*, 145, 80, doi: [10.1088/0004-6256/145/3/80](https://doi.org/10.1088/0004-6256/145/3/80)
- Du, B., Luo, A. L., Kong, X., et al. 2016, *ApJS*, 227, 27, doi: [10.3847/1538-4365/227/2/27](https://doi.org/10.3847/1538-4365/227/2/27)
- Duerbeck, H. W., & Rucinski, S. M. 2007, *AJ*, 133, 169, doi: [10.1086/509764](https://doi.org/10.1086/509764)
- Dvorak, S. W. 2006, *Information Bulletin on Variable Stars*, 5677, 1
- Eggen, O. J. 1979, *ApJS*, 41, 413, doi: [10.1086/190624](https://doi.org/10.1086/190624)
- Eggleton, P. P. 2012, *Journal of Astronomy and Space Sciences*, 29, 145, doi: [10.5140/JASS.2012.29.2.145](https://doi.org/10.5140/JASS.2012.29.2.145)
- Eggleton, P. P., & Kiseleva-Eggleton, L. 2001, *ApJ*, 562, 1012, doi: [10.1086/323843](https://doi.org/10.1086/323843)
- Eker, Z., Demircan, O., Bilir, S., & Karataş, Y. 2006, *MNRAS*, 373, 1483, doi: [10.1111/j.1365-2966.2006.11073.x](https://doi.org/10.1111/j.1365-2966.2006.11073.x)
- Eker, Z., Ak, N. F., Bilir, S., et al. 2008, *MNRAS*, 389, 1722, doi: [10.1111/j.1365-2966.2008.13670.x](https://doi.org/10.1111/j.1365-2966.2008.13670.x)
- Ekmekçi, F., Elmash, A., Yilmaz, M., et al. 2012, *NewA*, 17, 603, doi: [10.1016/j.newast.2012.03.001](https://doi.org/10.1016/j.newast.2012.03.001)
- Gaia Collaboration, Brown, A. G. A., Vallenari, A., et al. 2021, *A&A*, 649, A1, doi: [10.1051/0004-6361/202039657](https://doi.org/10.1051/0004-6361/202039657)
- Gao, X.-Y., Cai, Y.-W., Li, K., Gao, A., & Shao, Y.-D. 2022, *NewA*, 95, 101800, doi: [10.1016/j.newast.2022.101800](https://doi.org/10.1016/j.newast.2022.101800)
- Gazeas, K. D., Niarchos, P. G., Zola, S., Kreiner, J. M., & Rucinski, S. M. 2006, *AcA*, 56, 127. <https://arxiv.org/abs/0903.1364>
- Goderya, S. N., Leung, K. C., & Schmidt, E. G. 1996, *Ap&SS*, 246, 291, doi: [10.1007/BF00645645](https://doi.org/10.1007/BF00645645)
- . 1997, *Ap&SS*, 254, 295, doi: [10.1023/A:1000874329854](https://doi.org/10.1023/A:1000874329854)
- Goecking, K. D., & Duerbeck, H. W. 1993, *A&A*, 278, 463
- Green, G. M., Schlafly, E., Zucker, C., Speagle, J. S., & Finkbeiner, D. 2019, *ApJ*, 887, 93, doi: [10.3847/1538-4357/ab5362](https://doi.org/10.3847/1538-4357/ab5362)
- Henden, A. A., Templeton, M., Terrell, D., et al. 2016, *VizieR Online Data Catalog*, II/336
- Hilditch, R. W. 2001, *An Introduction to Close Binary Stars*
- Honková, K., Juryšek, J., Lehký, M., et al. 2014, *Open European Journal on Variable Stars*, 165, 1
- Horvat, M., Conroy, K. E., Pablo, H., et al. 2018, *ApJS*, 237, 26, doi: [10.3847/1538-4365/aacd0f](https://doi.org/10.3847/1538-4365/aacd0f)
- Hoňková, K., Juryšek, J., Lehký, M., et al. 2013, *Open European Journal on Variable Stars*, 160, 1
- Hu, K., Jiang, Z.-H., Yu, Y.-X., & Xiang, F.-Y. 2018, *NewA*, 62, 20, doi: [10.1016/j.newast.2018.01.002](https://doi.org/10.1016/j.newast.2018.01.002)
- Hubscher, J. 2005, *Information Bulletin on Variable Stars*, 5643, 1
- . 2013, *Information Bulletin on Variable Stars*, 6084, 1
- . 2014, *Information Bulletin on Variable Stars*, 6118, 1
- . 2015, *Information Bulletin on Variable Stars*, 6152, 1
- Hubscher, J., & Lehmann, P. B. 2012, *Information Bulletin on Variable Stars*, 6026, 1
- Hubscher, J., Lehmann, P. B., Monninger, G., Steinbach, H.-M., & Walter, F. 2010a, *Information Bulletin on Variable Stars*, 5918, 1
- . 2010b, *Information Bulletin on Variable Stars*, 5941, 1
- Hubscher, J., Paschke, A., & Walter, F. 2006, *Information Bulletin on Variable Stars*, 5731, 1
- Hubscher, J., Steinbach, H.-M., & Walter, F. 2008, *Information Bulletin on Variable Stars*, 5830, 1
- . 2009a, *Information Bulletin on Variable Stars*, 5874, 1
- . 2009b, *Information Bulletin on Variable Stars*, 5889, 1
- Hubscher, J., & Walter, F. 2007, *Information Bulletin on Variable Stars*, 5761, 1
- Hurley, J. R., Tout, C. A., & Pols, O. R. 2002, *MNRAS*, 329, 897, doi: [10.1046/j.1365-8711.2002.05038.x](https://doi.org/10.1046/j.1365-8711.2002.05038.x)
- Jayasinghe, T., Stanek, K. Z., Kochanek, C. S., et al. 2019, *MNRAS*, 486, 1907, doi: [10.1093/mnras/stz844](https://doi.org/10.1093/mnras/stz844)
- Jones, D., Conroy, K. E., Horvat, M., et al. 2020, *ApJS*, 247, 63, doi: [10.3847/1538-4365/ab7927](https://doi.org/10.3847/1538-4365/ab7927)
- Kaczmarek, T., Olczak, C., & Pfalzner, S. 2011, *A&A*, 528, A144, doi: [10.1051/0004-6361/201015233](https://doi.org/10.1051/0004-6361/201015233)
- Kemper, E. 1982, *AJ*, 87, 1395, doi: [10.1086/113229](https://doi.org/10.1086/113229)

- Kholopov, P. N., Samus, N. N., Kazarovets, E. V., & Perova, N. B. 1985, *Information Bulletin on Variable Stars*, 2681, 1
- Landin, N. R., Mendes, L. T. S., & Vaz, L. P. R. 2009, *A&A*, 494, 209, doi: [10.1051/0004-6361/20078403](https://doi.org/10.1051/0004-6361/20078403)
- Lee, J. W., & Park, J.-H. 2018, *PASP*, 130, 034201, doi: [10.1088/1538-3873/aaa390](https://doi.org/10.1088/1538-3873/aaa390)
- Li, F. X., Liao, W. P., Qian, S. B., et al. 2022, *ApJ*, 924, 30, doi: [10.3847/1538-4357/ac3425](https://doi.org/10.3847/1538-4357/ac3425)
- Li, K., Xia, Q.-Q., Kim, C.-H., et al. 2021a, *ApJ*, 922, 122, doi: [10.3847/1538-4357/ac242f](https://doi.org/10.3847/1538-4357/ac242f)
- Li, K., Xia, Q.-Q., Michel, R., et al. 2019, *MNRAS*, 485, 4588, doi: [10.1093/mnras/stz715](https://doi.org/10.1093/mnras/stz715)
- Li, K., Xia, Q.-Q., Kim, C.-H., et al. 2021b, *AJ*, 162, 13, doi: [10.3847/1538-3881/abfc53](https://doi.org/10.3847/1538-3881/abfc53)
- Li, L., Liu, Q., Zhang, F., & Han, Z. 2001, *AJ*, 121, 1091, doi: [10.1086/318731](https://doi.org/10.1086/318731)
- Li, L., & Zhang, F. 2006, *MNRAS*, 369, 2001, doi: [10.1111/j.1365-2966.2006.10462.x](https://doi.org/10.1111/j.1365-2966.2006.10462.x)
- Long, L., Zhang, L.-Y., Han, X. L., et al. 2019, *MNRAS*, 487, 5520, doi: [10.1093/mnras/stz1565](https://doi.org/10.1093/mnras/stz1565)
- Lucy, L. B. 1968, *ApJ*, 151, 1123, doi: [10.1086/149510](https://doi.org/10.1086/149510)
- Luo, A. L., Zhang, H.-T., Zhao, Y.-H., et al. 2012, *Research in Astronomy and Astrophysics*, 12, 1243, doi: [10.1088/1674-4527/12/9/004](https://doi.org/10.1088/1674-4527/12/9/004)
- Martignoni, M., Acerbi, F., & Barani, C. 2021, *NewA*, 84, 101512, doi: [10.1016/j.newast.2020.101512](https://doi.org/10.1016/j.newast.2020.101512)
- O'Connell, D. J. K. 1951, *Publications of the Riverview College Observatory*, 2, 85
- Özkardeş, B., & Erdem, A. 2012, *NewA*, 17, 143, doi: [10.1016/j.newast.2011.07.002](https://doi.org/10.1016/j.newast.2011.07.002)
- Papageorgiou, A., & Christopoulou, P. E. 2015, *AJ*, 149, 168, doi: [10.1088/0004-6256/149/5/168](https://doi.org/10.1088/0004-6256/149/5/168)
- Partovi, M., Abedi, A., & Roobiat, K. Y. 2021, *Serbian Astronomical Journal*, 203, 29, doi: [10.2298/SAJ2103029P](https://doi.org/10.2298/SAJ2103029P)
- Pavlenko, Y. V., Evans, A., Banerjee, D. P. K., et al. 2018, *A&A*, 615, A120, doi: [10.1051/0004-6361/201832717](https://doi.org/10.1051/0004-6361/201832717)
- Pecaut, M. J., & Mamajek, E. E. 2013, *ApJS*, 208, 9, doi: [10.1088/0067-0049/208/1/9](https://doi.org/10.1088/0067-0049/208/1/9)
- Pinto, G., & Romano, G. 1976, *Mem. Soc. Astron. Italiana*, 47, 229
- Pribulla, T., Chochol, D., & Vittone, A. A. 2003a, *Chinese Journal of Astronomy and Astrophysics Supplement*, 3, 361, doi: [10.1088/1009-9271/3/S1/361](https://doi.org/10.1088/1009-9271/3/S1/361)
- Pribulla, T., Kreiner, J. M., & Tremko, J. 2003b, *Contributions of the Astronomical Observatory Skalnaté Pleso*, 33, 38
- Pribulla, T., Rucinski, S. M., Conidis, G., et al. 2007, *AJ*, 133, 1977, doi: [10.1086/512772](https://doi.org/10.1086/512772)
- Pribulla, T., Vaňko, M., Chochol, D., Hambálek, Ľ., & Parimucha, Š. 2011, *Astronomische Nachrichten*, 332, 607, doi: [10.1002/asna.201111569](https://doi.org/10.1002/asna.201111569)
- Pribulla, T., Rucinski, S. M., Lu, W., et al. 2006, *AJ*, 132, 769, doi: [10.1086/505536](https://doi.org/10.1086/505536)
- Pribulla, T., Rucinski, S. M., Blake, R. M., et al. 2009, *AJ*, 137, 3655, doi: [10.1088/0004-6256/137/3/3655](https://doi.org/10.1088/0004-6256/137/3/3655)
- Prša, A., & Zwitter, T. 2005, *ApJ*, 628, 426, doi: [10.1086/430591](https://doi.org/10.1086/430591)
- Prša, A., Conroy, K. E., Horvat, M., et al. 2016, *ApJS*, 227, 29, doi: [10.3847/1538-4365/227/2/29](https://doi.org/10.3847/1538-4365/227/2/29)
- Pych, W., Rucinski, S. M., DeBond, H., et al. 2004, *AJ*, 127, 1712, doi: [10.1086/382105](https://doi.org/10.1086/382105)
- Qian, S. B., He, J. J., Soonthornthum, B., et al. 2008, *AJ*, 136, 1940, doi: [10.1088/0004-6256/136/5/1940](https://doi.org/10.1088/0004-6256/136/5/1940)
- Qian, S.-B., He, J.-J., Zhang, J., et al. 2017, *Research in Astronomy and Astrophysics*, 17, 087, doi: [10.1088/1674-4527/17/8/87](https://doi.org/10.1088/1674-4527/17/8/87)
- Qian, S. B., Yang, Y. G., Soonthornthum, B., et al. 2005, *AJ*, 130, 224, doi: [10.1086/430673](https://doi.org/10.1086/430673)
- Qian, S. B., Yuan, J. Z., Xiang, F. Y., et al. 2007, *AJ*, 134, 1769, doi: [10.1086/521927](https://doi.org/10.1086/521927)
- Qian, S. B., Zhang, J., He, J. J., et al. 2018, *ApJS*, 235, 5, doi: [10.3847/1538-4365/aaa601](https://doi.org/10.3847/1538-4365/aaa601)
- Qian, S. B., Zhang, J., Wang, J. J., et al. 2013, *ApJS*, 207, 22, doi: [10.1088/0067-0049/207/2/22](https://doi.org/10.1088/0067-0049/207/2/22)
- Qian, S. B., Jiang, L. Q., Fernández Lajús, E., et al. 2015, *ApJL*, 798, L42, doi: [10.1088/2041-8205/798/2/L42](https://doi.org/10.1088/2041-8205/798/2/L42)
- Rahman, A. 2000, *PASP*, 112, 123, doi: [10.1086/316485](https://doi.org/10.1086/316485)
- Ricker, G. R., Winn, J. N., Vanderspek, R., et al. 2015, *Journal of Astronomical Telescopes, Instruments, and Systems*, 1, 014003, doi: [10.1117/1.JATIS.1.1.014003](https://doi.org/10.1117/1.JATIS.1.1.014003)
- Rucinski, S. M. 1993, in *Astrophysics and Space Science Library*, Vol. 177, *Astrophysics and Space Science Library*, ed. J. Sahade, G. E. McCluskey, & Y. Kondo, 111, doi: [10.1007/978-94-011-2416-4_8](https://doi.org/10.1007/978-94-011-2416-4_8)
- Rucinski, S. M. 2006, *MNRAS*, 368, 1319, doi: [10.1111/j.1365-2966.2006.10207.x](https://doi.org/10.1111/j.1365-2966.2006.10207.x)
- Rucinski, S. M., Lu, W., Capobianco, C. C., et al. 2002, *AJ*, 124, 1738, doi: [10.1086/342341](https://doi.org/10.1086/342341)
- Rucinski, S. M., Lu, W., Mochnacki, S. W., Ogłóza, W., & Stachowski, G. 2001, *AJ*, 122, 1974, doi: [10.1086/323106](https://doi.org/10.1086/323106)
- Rucinski, S. M., Capobianco, C. C., Lu, W., et al. 2003, *AJ*, 125, 3258, doi: [10.1086/374949](https://doi.org/10.1086/374949)
- Rucinski, S. M., Pych, W., Ogłóza, W., et al. 2005, *AJ*, 130, 767, doi: [10.1086/431226](https://doi.org/10.1086/431226)
- Rucinski, S. M., Pribulla, T., Mochnacki, S. W., et al. 2008, *AJ*, 136, 586, doi: [10.1088/0004-6256/136/2/586](https://doi.org/10.1088/0004-6256/136/2/586)
- Samec, R. G., Chamberlain, H., Caton, D., et al. 2020, *JAAVSO*, 48, 150

- Sarotsakulchai, T., Qian, S. B., Soonthornthum, B., et al. 2018, *AJ*, 156, 199, doi: [10.3847/1538-3881/aadcf](https://doi.org/10.3847/1538-3881/aadcf)
- Schmidt, E. G. 1991, *AJ*, 102, 1766, doi: [10.1086/115999](https://doi.org/10.1086/115999)
- Schmidt, E. G., & Reiswig, D. E. 1993, *AJ*, 106, 2429, doi: [10.1086/116813](https://doi.org/10.1086/116813)
- Shappee, B. J., Prieto, J. L., Grupe, D., et al. 2014, *ApJ*, 788, 48, doi: [10.1088/0004-637X/788/1/48](https://doi.org/10.1088/0004-637X/788/1/48)
- Stepień, K. 2011, *A&A*, 531, A18, doi: [10.1051/0004-6361/201116689](https://doi.org/10.1051/0004-6361/201116689)
- Stickland, D. J., Koch, R. H., Pachoulakis, I., & Pfeiffer, R. J. 1994, *The Observatory*, 114, 107
- Strassmeier, K. G. 2009, *A&A Rv*, 17, 251, doi: [10.1007/s00159-009-0020-6](https://doi.org/10.1007/s00159-009-0020-6)
- Terrell, D., Munari, U., Zwitter, T., & Nelson, R. H. 2003, *AJ*, 126, 2988, doi: [10.1086/379678](https://doi.org/10.1086/379678)
- Terrell, D., & Wilson, R. E. 2005, *Ap&SS*, 296, 221, doi: [10.1007/s10509-005-4449-4](https://doi.org/10.1007/s10509-005-4449-4)
- Tian, X.-m., Zhu, L.-y., & Wang, Z.-h. 2019, *PASP*, 131, 084203, doi: [10.1088/1538-3873/ab221e](https://doi.org/10.1088/1538-3873/ab221e)
- Twigg, L. W. 1979, *MNRAS*, 189, 907, doi: [10.1093/mnras/189.4.907](https://doi.org/10.1093/mnras/189.4.907)
- Tylenda, R., Hajduk, M., Kamiński, T., et al. 2011, *A&A*, 528, A114, doi: [10.1051/0004-6361/201016221](https://doi.org/10.1051/0004-6361/201016221)
- Wadhwa, S. S., De Horta, A., Filipović, M. D., et al. 2021a, *MNRAS*, 501, 229, doi: [10.1093/mnras/staa3637](https://doi.org/10.1093/mnras/staa3637)
- Wadhwa, S. S., Tothill, N. F. H., DeHorta, A. Y., & Filipović, M. 2021b, *Research in Astronomy and Astrophysics*, 21, 235, doi: [10.1088/1674-4527/21/9/235](https://doi.org/10.1088/1674-4527/21/9/235)
- Wang, S.-G., Su, D.-Q., Chu, Y.-Q., Cui, X., & Wang, Y.-N. 1996, *ApOpt*, 35, 5155, doi: [10.1364/AO.35.005155](https://doi.org/10.1364/AO.35.005155)
- Wilson, R. E. 1979, *ApJ*, 234, 1054, doi: [10.1086/157588](https://doi.org/10.1086/157588)
- . 1990, *ApJ*, 356, 613, doi: [10.1086/168867](https://doi.org/10.1086/168867)
- . 1994, *PASP*, 106, 921, doi: [10.1086/133464](https://doi.org/10.1086/133464)
- Wilson, R. E., & Devinney, E. J. 1971, *ApJ*, 166, 605, doi: [10.1086/150986](https://doi.org/10.1086/150986)
- Wolf, M., Molík, P., Hornoch, K., & Šarounová, L. 2000, *A&AS*, 147, 243, doi: [10.1051/aas:2000300](https://doi.org/10.1051/aas:2000300)
- Yaşarsoy, B., & Yakut, K. 2013, *AJ*, 145, 9, doi: [10.1088/0004-6256/145/1/9](https://doi.org/10.1088/0004-6256/145/1/9)
- Yakut, K., & Eggleton, P. P. 2005, *ApJ*, 629, 1055, doi: [10.1086/431300](https://doi.org/10.1086/431300)
- Yakut, K., Kalomeni, B., & İbanoğlu, C. 2004, *A&A*, 417, 725, doi: [10.1051/0004-6361:20031773](https://doi.org/10.1051/0004-6361:20031773)
- Yang, Y.-G., & Qian, S.-B. 2015, *AJ*, 150, 69, doi: [10.1088/0004-6256/150/3/69](https://doi.org/10.1088/0004-6256/150/3/69)
- Yang, Y. G., Qian, S. B., & Zhu, L. Y. 2005a, *AJ*, 130, 2252, doi: [10.1086/496880](https://doi.org/10.1086/496880)
- Yang, Y.-G., Qian, S.-B., Zhu, L.-Y., He, J.-J., & Yuan, J.-Z. 2005b, *PASJ*, 57, 983, doi: [10.1093/pasj/57.6.983](https://doi.org/10.1093/pasj/57.6.983)
- Yıldırım, M. F., & Soyduğan, F. 2017, in *American Institute of Physics Conference Series*, Vol. 1815, Turkish Physical Society 32nd International Physics Congress, 080025, doi: [10.1063/1.4976457](https://doi.org/10.1063/1.4976457)
- Zhang, L.-Y., Long, L., Shi, J., et al. 2020, *MNRAS*, 495, 1252, doi: [10.1093/mnras/staa942](https://doi.org/10.1093/mnras/staa942)
- Zhao, E., Qian, S., Li, L., et al. 2014, *NewA*, 26, 112, doi: [10.1016/j.newast.2013.07.006](https://doi.org/10.1016/j.newast.2013.07.006)
- Zheng, S.-Y., Li, K., & Xia, Q.-Q. 2021, *MNRAS*, 506, 4251, doi: [10.1093/mnras/stab1829](https://doi.org/10.1093/mnras/stab1829)
- Zhou, X., Qian, S. B., Zhang, J., Zhang, B., & Kreiner, J. 2016, *AJ*, 151, 67, doi: [10.3847/0004-6256/151/3/67](https://doi.org/10.3847/0004-6256/151/3/67)
- Zhu, L. Y., Qian, S. B., Soonthornthum, B., He, J. J., & Liu, L. 2011, *AJ*, 142, 124, doi: [10.1088/0004-6256/142/4/124](https://doi.org/10.1088/0004-6256/142/4/124)
- Zhu, L. Y., Qian, S. B., Soonthornthum, B., & Yang, Y. G. 2005, *AJ*, 129, 2806, doi: [10.1086/430187](https://doi.org/10.1086/430187)
- Zhu, L.-Y., Zhao, E.-G., & Zhou, X. 2016, *Research in Astronomy and Astrophysics*, 16, 68, doi: [10.1088/1674-4527/16/4/068](https://doi.org/10.1088/1674-4527/16/4/068)
- Zola, S., Rucinski, S. M., Baran, A., et al. 2004, *AcA*, 54, 299
- Zwitter, T., Munari, U., Marrese, P. M., et al. 2003, *A&A*, 404, 333, doi: [10.1051/0004-6361:20030446](https://doi.org/10.1051/0004-6361:20030446)